Functionality and Functionalization of Metal—Organic Frameworks

by

Jake Andrew Boissonnault

A dissertation submitted in partial fulfillment
of the requirements for the degree of
Doctor of Philosophy
(Chemistry)
in The University of Michigan
2018

Doctoral Committee:

Professor Adam J. Matzger, Chair
Professor Bart M. Bartlett
Professor Michael J. Solomon
Assistant Professor Markos Koutmos

Jake A. Boissonnault

jboisson@umich.edu

ORCID iD: 0000-0003-1299-1860

“When you find yourself in a hole, stop digging.”

-W. Rogers

Acknowledgements

I would like to thank first and foremost my advisor for the past 4~ish years, Professor Adam J. Matzger. He has provided me with so much that words cannot encompass the gratitude and thankfulness I have for him. Even when things looked bleak, he still believed that it could be turned around with the right attitude and perseverance. He has been an amazing mentor and it is my hope that I can do him proud in my future endeavors.

I would also like to thank my committee members, Professor Bart M. Bartlett, Professor Michael J. Solomon, Professor Markos Koutmous, and Professor Mark M. Banaszak Holl, whom have provided great feedback and ensured that I was on the right track for success.

Further, I would be remiss not to include Dr. Antek G. Wong-Foy in the list of people who have been extremely influential of my time here. He is not only indispensable and irreplaceable in the lab, but he has also been very reliable and always willing to help out as long as you were willing to be helped out. My time here would have been significantly more difficult without Antek's know-how and for that I am very grateful.

I also have to thank the rest of the Matzger Lab past and present. They are all like family to me and they have all made my time here memorable. Dr. Ping Guo who was my first desk-mate and helped to show me the ropes. Dr. Laura Pfund who taught me the most useful technique in the lab, Raman. Dr. Ananya Dutta who was always great to talk to about science and anything. Dr. Jon Bennion, you were a great friend while you were here, all the times spent playing board games and chilling. Dr. Kyle McDonald you are absolutely fabulous and were always eager to talk shop. Dr. Jialiu Ma my lunch buddy, lab buddy and soon to be Intel work buddy, I'm glad that I got to know you. Dr. Kortney Kersten the voice of reason yelling at me to get stuff done, in the end I am grateful for that. Rosalyn who was the best deskmate. All the talks with Ren about cool science. And all of the "youngins", you have all been great for just the science talk, chatting, being good labmates. I'm glad to have counted you all amongst my friends.

To all my friends outside the Matzger lab, Dr. Sam Esarey, the Kyles, both Williams and Dr. Fergueson, the "other" Dr. Jake, Dr. Nate Ulrich and Molly, Isabel, Samson, Chauncey, Izzy, Reese, Luna, and Emily. You all have been so great. We've had so many good experiences, playing board games, watching the Steelers lose, attempting to get through a birthday night out without ending up at Denny's, Pathfinder. You guys and gals are all really the best. And Sam and Kyle, I'll keep the Kraken waiting.

To Professor Seth M. Cohen who saw potential in me all those years ago. I would literally not be where I am now if you hadn't given me the amazing opportunity to work in your lab.

My dad, mom, and sister who have supported me throughout everything. I am excited that after all this time apart, we'll be close together again. Thank you so much for all of your undying support.

And Jessica. Thank you for putting up with me through literally everything. It's been a tough 5 years living so far away from you. I'm looking forward to never having to be apart from you again. I love you so much.

Table of Contents

List of Figures

List of Tables

Abstract

Metal—organic frameworks (MOFs) are a relatively new class of materials based upon organic linkers bridging metal clusters or ions to create a 2D or 3D structure. The most exceptional materials among MOFs possess large surface areas extending up to 6000 m^2/g and are geared towards applications in gas storage, separations, and catalysis. In these applications, the chemical environment of the MOF interior is important as it can allow for selective interactions with guests as necessary. In the functionalization of MOFs, postsynthetic exchange (PSE), a suite of methods for introducing chemical functionality to a preformed MOF, has arisen as a key method for incorporation of new functional groups into MOFs that allow for further tailoring of these materials towards applications. This dissertation explores the use of functional environments in MOFs towards applications in separation and probes the mechanism of PSE in MOFs and the effects this has on the chemical environment. Chapter 2 describes the utility of MOFs with coordinatively unsaturated metal centers for purification of the industrially important gas chloromethane; this was achieved through selective interactions with the impurity dimethyl ether thus offering an alternative to the current practice of reactive separation. The MOFs, HKUST-1, MIL-100(Fe), and Co/DOBDC showed not only high capacities for dimethyl ether adsorption, but Co/DOBDC was shown to be easily regenerable with mild heating under a flow of inert gas. Chapter 3 describes mechanistic studies of how PSE effects the chemical environment inside the MOF. The microstructure of MOFs after PSE was examined using Raman microscopy which revealed exchanged ligand was concentrated at the edges of the crystal and decreased in concentration towards the center of the crystal resulting in a gradient core-shell behavior. Diffusion studies of carboxylate based ligands into MOF-5 showed that lack of uniform exchange is the result of slow diffusion kinetics. This core-shell behavior was also observed in UiO-66 and UMCM-8 showing the general applicability of PSE in generating core-shell materials. Finally, in Chapter 4 PSE methods were applied in a different class of MOFs, zeolitic imidazolate frameworks, to incorporate a primary amine in order to increase the CO_2

uptake of the material. By using the readily available biomolecule histamine, incorporation into ZIF-8 saw a marked increase in CO_2 capacity compared to the unmodified material.

Chapter 1

Introduction

1.1 Metal—Organic Frameworks

Metal-organic frameworks (MOFs or MCPs) are a class of 2D or 3D coordination polymers composed of polytopic organic linkers bridging metal clusters or metal ions.[1] It is also common for MOFs to exhibit permanent porosity upon removal of guests from within. Compared to other porous materials (e.g. alumina, silica gel, activated carbon, zeolites), MOFs represent a relatively new class of materials with origins dating back to the synthesis of an infinite polymeric framework by Robson and coworkers in 1989.[2] Robson's framework consisted of Cu^{1+} ions bridged by the tetrahedral 4,4′,4″,4‴-tetracyanotetraphenylmethane to form a diamondoidal lattice with large cavities present in the lattice, though upon removal of guests all potential porosity was lost (Figure 1.1). Synthesis of new coordination polymers followed Robson's initial success though a permanently porous material had yet to be synthesized.[3,4] This changed in 1999 with the near simultaneous publishing of two distinctly different permanently porous coordination polymers that would become the first members of what became generally known as MOFs: HKUST-1 was synthesized by Williams and MOF-5 by Yaghi.[5,6] HKUST-1 and MOF-5 both possessed high surface areas when compared to silica and alumina that could, at maximum surface area, barely crest 1000 m^2/g with HKUST-1 at 692 $m^2/$ and MOF-5 at a staggering 2900 m^2/g upon removal of guests, a process that has become known as activation (Figure 1.2). These two materials laid the groundwork for what would become the burgeoning field of MOFs and it should be noted that with the development of synthesis conditions and activation methods for HKUST-1 and MOF-5 that the surface area of the materials has been reported to maximums of 1840 m^2/g and 3800 m^2/g, respectively.[7,8] Since these first reports, hundreds of new MOF structure types have been discovered and many thousands of papers published on these new structures and their applications. These efforts have yielded MOFs that possess surface areas in excess of 6000 m^2/g, extremely low densities, and promise in applications that range from adsorption and storage of fuel gases such as hydrogen and methane,

sequestration and separation of CO_2 and water from air streams, heterogeneous catalysis, and sensing.[9-17]

1.2 Synthesis and Design of MOFs

MOFs are composed of metal clusters or metal ions bridged by organic linkers with multiple metal binding groups (e.g. benzene-1,4-dicarboxylate and benzene-1,3,5-tricarboxylate). The most common metal cluster motifs revolve around a number of known acetate metal clusters such as basic zinc acetate and metal paddlewheels. As such, the most common linkers in MOF synthesis have tended to be rigid polycarboxylates. In the example of MOF-5 above, the basic zinc acetate cluster is bridged by terephthalate units creating a cubic structure. Other linear dicarboxylates used in place of terephthalic acid in the synthesis will yield MOFs with the same connectivity as MOF-5 but with different features such as pendant functional groups or larger pores.[18] Using this method, a series of isostructural MOFs can be synthesized. If however, a linker with a different connectivity such as 1,3,5-tris(4-carboxyphenyl)benzene is used with the same conditions as MOF-5, an entirely new structure is made.[19] It is through the combination of various metal clusters and linker connectivities that a large number of different MOF structures can be synthesized before even considering the addition of other linkers such as 4,4′-bypyridine, imidazolates, or even other carboxylates.[20-22] This can lead to MOFs with varying pore geometries and sizes as well as different metal coordination environments that can result in an auxiliary ligand coordinated to the metal center that can be removed, leaving a coordinatively unsaturated metal center.

In addition to the choice of linkers and metal clusters, it is possible to introduce chemical functionalities on the linkers used in the synthesis resulting in a MOF adorned with these functionalities. Using this method for chemical functionalization limits the types of groups that can be incorporated. This is due to the specific requirements for the synthesis of the MOF which necessitate that any pendant functionalities on linkers be stable to the solvothermal synthesis conditions and not interfere with the formation of the metal cluster and thus the MOF formation. These considerations eliminate thermally sensitive functional groups. Additionally, in some MOF syntheses functional groups can interfere with metal cluster formation preventing successful MOF synthesis. Groups that tend to be problematic are those that can act as metal coordinating groups such as alcohols, aliphatic amines, and thiols, though some MOFs have no

issue with incorporation of these groups. The incorporation of aryl amines, halogens, amides, nitriles, alkenes, and alkynes has been successfully achieved with MOF synthesis from linkers functionalized with these groups although the success is dependent on the metals, ligand substitution, and synthetic conditions.[23-26]

1.3 Postsynthetic Modification of MOFs

In an effort to expand the scope of functional groups that can be incorporated into MOFs, different synthetic strategies have been developed. These methods involve subjecting synthesized MOFs to chemical reactions altering the existing chemical groups. As they occur after synthesis, these methods are referred to as postsynthetic modification (PSM). The first PSM reactions were simple proof of concept reactions involving the transformation of pendant aryl amines in MOFs to amides through reaction with acid anhydrides. Specifically, Cohen and coworkers showed that reaction of pendant amines in IRMOF-3 with acetic anhydride yielded the acetamide (Figure 1.3).[27] Since this work, the scope and kinds of reactions for PSM have greatly expanded to allow for the incorporation of a variety of functional groups such as ureas, thioureas, alcohols, alkylamines, thiols, catechols, and azides.[28-30] In addition, the types of reactions that can be conducted on MOFs has been greatly expanded and includes "click", S_N2, epoxidation, nitration, and reduction reactions.[29-31] PSM for deprotection of functional groups has also been conducted allowing for another method of functionalization. In work by Telfer and coworkers, an IRMOF-10 derivative bearing a boc-protected L-proline moiety was synthesized and successfully deprotected through heating of the sample in N,N-dimethylformamide revealing the secondary amine that was then used for catalysis.[32] Salt exchange reactions also provide another method of PSM to allow for the incorporation of charged species into a charged MOF. In work by Genna *et al.*, the counter cation in the anionic MOF ZJU-28 was replaced with a cationic transition-metal catalyst.[33] Though the possibilities for functional group incorporation through PSM are virtually limitless, the reaction conditions are the primary limiting factor as the MOF used in the reaction must be stable to these conditions to render the desired final material with the desired functional groups.

1.4 Postsynthetic Exchange in MOFs

A more recent method for functionalization of MOFs has relied on the direct replacement of linkers in the MOF with similar functionalized linkers with the same connectivity. This idea

can be traced back to coordination chemistry and indeed back to the synthesis of Robson's material which involved the replacement of acetonitrile ligands in $[Cu(CH_3CN)_4]BF_4$ with the linker tetracyanotetraphenylmethane. Direct replacement of linkers and metals in MOFs after synthesis through exchange in solution is fairly recent, and has only come about in 2009 with work by Kim and coworkers where Cd^{2+} ions in the metal cluster were replaced with Pb^{2+} ions in solution.[34] Ligand exchange studies in MOFs were first conducted in 2011 by three different groups each showing in three distinct MOFs with three distinct linker types (bipyridines, terephthalates, and imidazolates) that direct replacement of MOF linkers was possible by contacting the MOF with a solution containing the dissolved ligand (Figure 1.4).[35-37] While originally only applicable to a few MOFs, postsynthetic exchange (PSE, also known as solvent-assisted linker/metal exchange or stepwise synthesis) has been applied to numerous MOF systems allowing for greater options in functionalization. PSE is typically conducted with the MOF in a polar solution containing a functional group-bearing linker with the same connectivity as the linker originally present in the MOF. After gentle agitation of the MOF with either heating or at room temperature, the resulting MOF will have the new linker incorporated, displacing some or all of the original linker in the process. The amount of exchange in the MOF is dependent on the equivalents of the linker in solution relative to the linker in the MOF where complete exchange is typically only achieved when large excess (>10 equivalents) is used. Additionally, the equilibrium can be driven towards the new linker by replacing the solution after a certain amount of time has passed, ensuring that the new linker is in constant excess. In an example by Hupp and coworkers, a parent MOF, $Zn_2(tmbdc)_2(bpy)$, was subjected to sequential PSE reactions replacing every initial component with new linkers and metals creating a new material, $Ni_2(2,6\text{-ndc})_2(dabco)$, that maintained the same connectivities of the parent but could not be obtained through standard solvothermal methods.[38] This method of complete linker exchange has also been utilized by the Rosi group to synthesize a series of extended MOFs through replacement of 2,6-naphthalenedicarboxylate in bio-MOF-101 with biphenyl-4,4′-dicarboxyate, azobenzene-4,4′-dicarboxylate, or 2′-amino-1,1′:4,1″-terphenyl-4,4″-dicarboxylate to yield bio-MOF-100, -102, or -103, respectively.[39] It is interesting to note in this case and a few others that PSE of linkers possessing different lengths is possible allowing for the pore size of a synthesized MOF to be expanded or contracted through PSE. Low levels of incorporation can occur if there is some steric or electronic effect of functional groups on the new linker that

inhibit or slow incorporation or if the ratio of new linker to MOF is close to 1:1. This allows for a way to create two different materials with varying degrees of incorporation depending on the ratio of linker in solution with each material having different desirable properties. In particular, low levels of incorporation may be of interest for loading of catalysts into MOFs.

1.5 Separations in MOFs

Aside from gas storage applications of MOFs, separations are another prominent area of study.[40,41] This is due to the high surface area of MOFs that allows for high adsorption capacity and the chemical tunability that allows for specific interactions between MOFs and particular guests. Additionally, high surface area of the MOFs allowing for a larger amount of a mixture to be separated or purified relative to silica or alumina and the regeneration of MOFs tends to be facile requiring only mild heating under flowing N_2 or dynamic vacuum. This has allowed for MOFs to be usable in the separations of molecules with different chemical functionalities. This has allowed for separations of olefins from paraffins, water from air, oxygen from air, H_2 from syn gas, and CO_2 from air or flue gas streams.[15,42-44] In all of these cases, every tool available to the MOF chemist has been utilized including activation to reveal coordinatively unsaturated metal centers, PSM, and linker design. In work by Caskey *et al.*, the MOF series M/DOBDC (M = Co, Ni, Zn, or Mg) was shown to possess high selectivity for CO_2 over N_2 allowing for removal of CO_2 from a gaseous mixture passed over the MOF.[43] This is suspect to be in large part due to the coordinatively unsaturated metal centers that are present in the activated MOF which can selectively coordinate CO_2 over N_2. Long and coworkers have shown that by modifying a similar material known as M_2(DOBPDC) (M = Mg, Mn, Fe, Co, Ni, or Zn) with diamines at the coordinatively unsaturated metal center before CO_2 separation, that capacity for CO_2 can be greatly increased compared to the unmodified material.[46] Fischer and coworkers showed that in a flexible DMOF-1 derivative adorned with alkyl ethers selective CO_2 adsorption could be attained.[47] The activated MOF, $[Zn_2(BME\text{-}bdc)_2(dabco)]_n$, would exist in a nonporous state with no uptake of nitrogen observed but would, upon increasing partial pressure of CO_2, exhibit porosity and selectively uptake CO_2. Liquid separations have also been examined in MOFs utilizing the same principles as the separations above. Millange and coworkers showed that MIL-53(Fe) could be used in the separation of a variety of alkyl benzenes including separation of the three regioisomers of xylene.[48] Kaskel and coworkers also showed that by using

a terephthalic acid ligand modified with a chiral functional group, the corresponding chiral MOF, chir-UMCM-1, can be synthesized and utilized for the liquid phase separation of a racemic compound, in this case 1-phenylethanol.[49]

1.6 Organization of Thesis

This thesis focuses on functionalization of MOFs and the use of functionalized MOFs in gas sorption applications. Chapter 2 examines the potential use of MOFs in the adsorptive separation of a gaseous mixture of methyl chloride and dimethyl ether. Methyl chloride is a commodity chemical used in the production of silicones synthesized through hydrochlorinolysis of methanol. During the reaction, a side reaction of the product methyl chloride with methanol yields dimethyl ether which cannot be removed from the mixture by conventional means of distillation and is instead removed by reactive separation by passing the gaseous mixture over a column of >96% sulfuric acid. Since a chemical difference between the two molecules is utilized in the reactive separation, MOFs will be shown to be able to take advantage of this with coordinatively unsaturated metal centers allowing for selective adsorption of dimethyl ether.

In Chapter 3, the microstructure of MOFs after PSE is examined in systems where complete exchange does not occur. PSE where low loading is desired, such as catalysis, has previously relied on the assumption that exchange occurs uniformly throughout the material even though this had not been studied extensively and there was little data to back this assumption. Through Raman microscopy of cross-sectioned MOF-5 crystals after PSE, the distribution of linkers through the MOF is shown to occur in an out-to-in fashion with exchange occurring preferentially at the surface extending toward the center with time.

Chapter 4 shows the efforts to incorporate a readily biosynthesizable molecule, histamine, into MOFs possessing imidazolate as linkers. Incorporation of histamine into the MOF ZIF-8 occurs readily at room temperature with up to 50% incorporation after 18 hours. This material shows improved CO_2 uptake compared to the parent ZIF-8, though with significantly diminished kinetics. Progress toward incorporation of histamine into larger pore MOFs will be discussed along with remaining challenges.

1.7 Figures

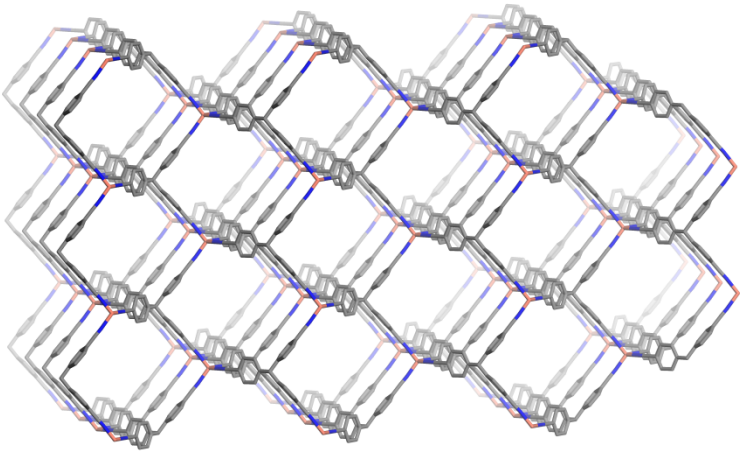

Figure 1.1. Structure of Cu(4,4′,4″,4‴-tetracyanotetraphenylmethane)[BF_4] as discovered by Robson and coworkers.[2]

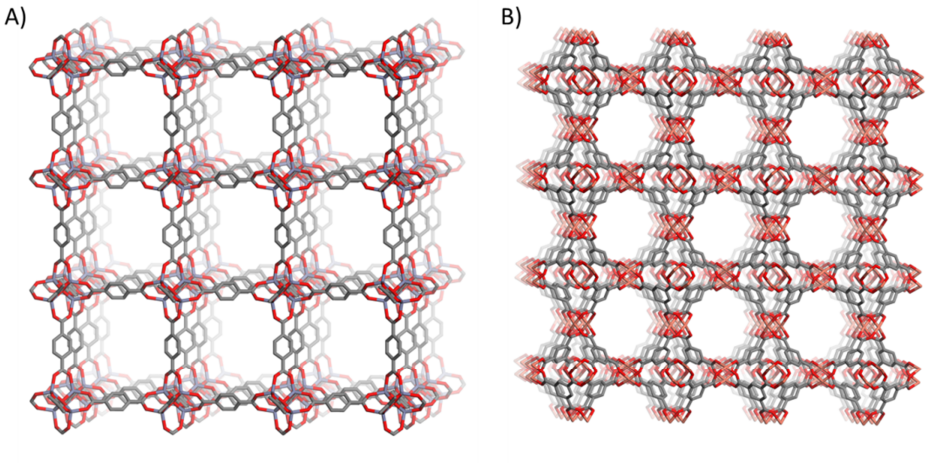

Figure 1.2. Structures of MOF-5 (Zn_4O(terephthalate)$_3$) and HKUST-1 (Cu_3BTC_2, HKUST = Hong Kong University of Science and Technology) as discovered by the groups of Yaghi and Williams, respectively.[5,6]

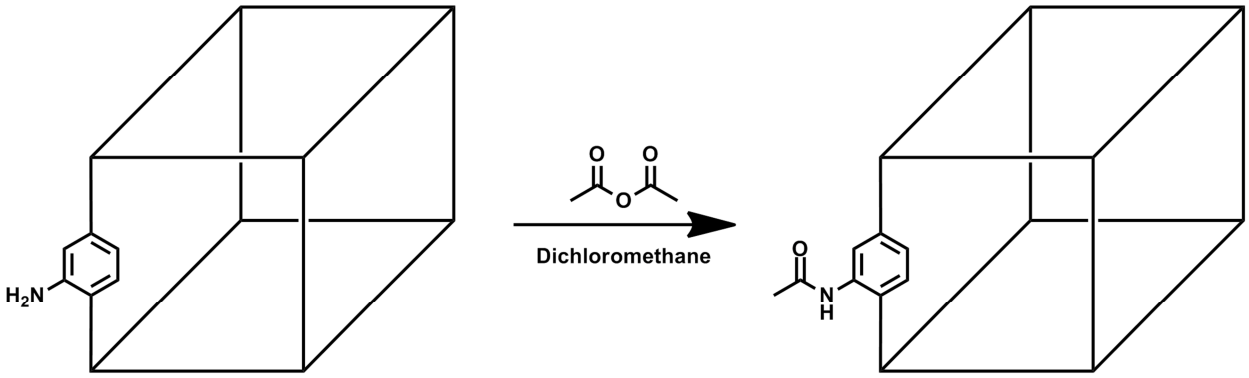

Figure 1.3. Schematic of the initial PSM reaction carried out by Cohen and coworkers on formed crystals of IRMOF-3 (IRMOF = Isoreticular MOF).

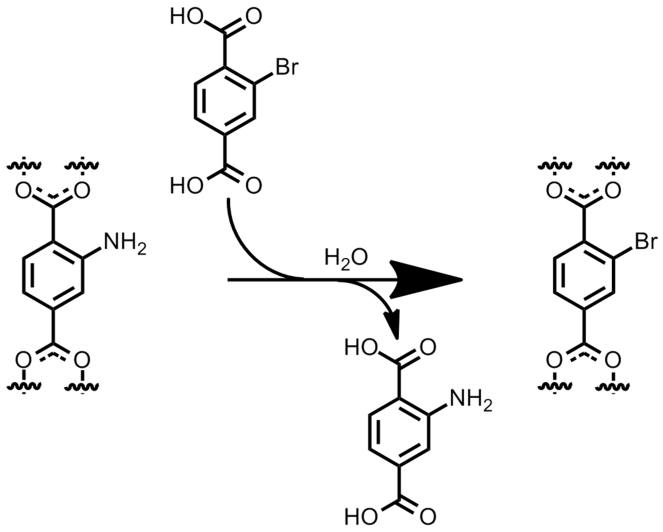

Figure 1.4. Schematic of ligand exchange in MOFs.

1.8 References

1) Seth, S. Matzger, A. J. Metal—Organic Frameworks: Examples, Couterexamples, and an Actionable Definition. *Cryst. Growth Des.* **2017**, *17*, 4043-4048.

2) Hoskins, B. F.; Robson, R. Infinite polymeric frameworks consisting of three dimensionally linked rod-like segments. *J. Am. Chem. Soc.* **1989**, *111*, 5962-5964.

3) Abrahams, B. F.; Hoskins, B. F.; Robson, R. A New Type of Infinite 3D Polymeric Network Containing 4-Connected, Peripherally-Linked Metalloporphyrin Building Blocks. *J. Am. Chem. Soc.* **1991**, *113*, 3606-3607.

4) Kuroda-Sowa, T.; Yamamoto, M.; Munakata, M.; Seto, M.; Maekawa, M. Three-fold Interpenetrating Diamondoid Frameworks with π—π Stacking of Alternated Coordinated and Uncoordinated Ligands: Crystal Structures of Copper(I) Coordination Compounds, [Cu(DMTPN)2]X(DMTPN)(thf) (DMPTN = 2,5-Dimethylterephthalonitrile; X = BF4, ClO4). *Chem. Lett.* **1996**, 349-350.

5) Chui, S. S.-Y.; Lo, S. M.-F.; Charmant, J. P. H.; Orpen, A. G.; Williams, I. D. A Chemically Functionalizable Nanaporous Material [Cu3(TMA)2(H2O)3]n. *Science* **1999**, *283*, 1148-1150.

6) Li, H.; Eddaoudi, M.; O'Keeffe, M.; Yaghi, O. M. Design and synthesis of an exceptionally stable and highly porous metal-organic framework. *Nature* **1999**, *402*, 276-279.

7) Kayne, S. S.; Dailly, A.; Yaghi, O. M.; Long, J. R. Impact of Preparation and Handling on the Hydrogen Storage Properties of Zn4O(1,4-benzenedicarboxylate)3 (MOF-5). *J. Am. Chem. Soc.* **2007**, *129*, 14176-14177.

8) Peng, Y.; Krungleviciute, V.; Eryazici, I.; Hupp, J. T.; Farha, O. K.; Yildirim, T. Methane Storage in Metal—Organic Frameworks: Current Records, Surprise Findings, and Challenges. *J. Am. Chem. Soc.* **2013**, *135*, 11887-11894.

9) Farha, O. K.; Eryazici, I.; Jeong, N. C.; Hauser, B. G.; Wilmer, C. E.; Sarjeant, A. A.; Snurr, R. Q. Nguyen, S. T.; Yazaydin, A. O.; Hupp, J. T. Metal—Organic Framework Materials with Ultrahigh Surface Areas: Is the Sky the Limit?. *J. Am. Chem. Soc.* **2012**, *134*, 15016-15021.

10) Li. P; Nicolaas, A. V.; Malliakas, C. D.; Gomez-Gualdron, D. A.; Howarth, A. J.; Mehdi, B. L.; Dohnalkova, A.; Browning, N. D.; O'Keeffe, M.; Farha, O. K. Bottoms-up construction of a superstructure in a porous uranium-organic crystal. *Science* **2017**, *356*, 624-627.

11) He, Y.; Zhou, W.; Qian, G.; Chen, B. Methane storage in metal—organic frameworks. *Chem. Soc. Rev.* **2014**, *43*, 5657-5678.

12) Suh, M. P.; Park, H. J.; Prasad, T. K.; Lim, D.-W. Hydrogen Storage in Metal—Organic Frameworks. *Chem. Rev.* **2012**, *112*, 782-835.

13) Trickett, C. A.; Helal, A.; Al-Maythalony, B. A.; Yamani, Z. H.; Cordova, K. E.; Yaghi, O. M. The chemistry of metal—organic frameworks for CO2 capture, regeneration and conversion. *Nature Reviews Materials* **2017**, *2*, 17045.

14) Sumida, K.; Rogow, D. L.; Mason, J. A.; McDonald, T. M.; Bloch, E. D.; Herm, Z. R.; Bae, T.-H.; Long, J. R. Carbon Dioxide Capture in Metal—Organic Frameworks. *Chem. Rev.* **2012**, *112*, 724-781.

15) Guo, P; Wong-Foy, A. G.; Matzger, A. J. Microporous Coordination Polymers as Efficient Sorbents for Air Dehumidification. *Langmuir* **2014**, *30*, 1921-1925.

16) Huang, Y.-B.; Liang, J.; Wang, X.-S.; Cao, R. Mulitfunctional metal—organic framework catalysts: synergistic catalysis and tandem reactions. *Chem. Soc. Rev.* **2017**, *46*, 126-157.

17) Lustig, W. P.; Mukherjee, S.; Rudd, N. D.; Desai, A. V.; Li, J.; Ghosh, S. K. Metal—organic frameworks: functional luminescent and photonic materials for sensing applications. *Chem. Soc. Rev.* **2017**, *46*, 3242-3285.

18) Eddaoudi, M.; Kim, J.; Rosi, N.; Vodak, D.; Wachter, J.; O'Keeffe, M.; Yaghi, O. M. Systematic Design of Pore Size and Functionality in Isoreticular MOFs and Their Application in Methane Storage. *Science* **2002**, *295*, 469-472.

19) Chae, H. K.; Siberio-Perez, D. Y.; Kim, J.; Go, Y.; Eddaoudi, M.; Matzger, A. J.; O'Keeffe, M.; Yaghi, O. M. A Route to High Surface Area, Porosity and Inclusion of Large Molecules in Crystals. *Nature* **2004**, *427*, 523-527.

20) Koh, K.; Wong-Foy, A. G.; Matzger, A. J. A Crystalline Mesoporous Coordination Copolymer with High Microporosity. *Angew. Chem. Int. Ed.* **2008**, *47*, 677-680.

21) Dau, P. V.; Kim, M.; Garibay, S. J.; Munch, F. H. L.; Moore, C. E.; Cohen, S. M. Single-Atom Ligand Changes Affect Breathing in an Extended Metal—Organic Framework. *Inorg. Chem.* **2012**, *51*, 5671-5676.

22) Huang, X.-C.; Lin, Y.-Y.; Zhang, J.-P.; Chen, X.-M. Ligand-Directed Strategy for Zeolite-Type Metal—Organic Frameworks: Zinc(II) Imidazolates with Unusual Zeolitic Topologies. *Angew. Chem. Int. Ed.* **2006**, *45*, 1557-1559.

23) Xiong, S.; He, Y.; Krishna, R.; Chen, B.; Wang, Z. Metal—Organic Framework with Functional Amide Groups for Highly Selective Gas Separation. *Cryst. Growth Des.* **2013**, *13*, 2670-2674.

24) Kim, M.; Garibay, S. J.; Cohen, S. M. Microwave-Assisted Cyanation of an Aryl Bromide Directly on a Metal—Organic Framework. *Inorg. Chem.* **2011**, *50*, 729-731.

25) Dong, M.-J.; Zhao, M.; Ou, S.; Zou, C.; Wu, C.-D. A Luminescent Dye@MOF Platform: Emission Fingerprint Relationships of Volatile Organic Molecules. *Angew. Chem. Int. Ed.* **2013**, *53*, 1575-1579.

26) Tran, L. D.; Feldblyum, J. I.; Wong-Foy, A. G.; Matzger, A. J. Filling Pore Space in a Microporous Coordination Polymer to Improve Methane Storage Performance. *Langmuir* **2015**, *31*, 2211-2217.

27) Wang, Z.; Cohen, S. M. Postsynthetic Covalent Modification of a Neutral Metal—Organic Framework. *J. Am. Chem. Soc.* **2007**, *129*, 12368-12369.

28)Volkringer, C.; Cohen, S. M. Generating Reactive MILs: Isocyanate and Isothiocyanate—bearing MILs through Postsynthetic Modification. *Angew. Chem. Int. Ed.* **2010**, *49*, 4644-4648.

29) Savonnet, M.; Bazer-Bachi, D.; Bats, N.; Perez-Pellitero, J.; Jeanneau, E.; Lecocq, V.; Pinel, C.; Farrusseng, D. Generic Postfunctionalization Route from Amino-Derived Metal—Organic Frameworks. *J. Am. Chem. Soc.* **2010**, *132*, 4518-4519.

30) Kronast, A.; Eckstein, S.; Altenbuchner, P. T.; Hendelang, K.; Vagin, S. I.; Reiger, B. Gated Channels and Selectivity Tuning of CO2 over N2 Sorption by Post-Synthetic Modification of a UiO-66-Type Metal—Organic Framework. *Chem. Eur. J.* **2016**, *22*, 12800-12807.

31) Bernt, S.; Guillerm, V.; Serre, C.; Stock, N. Direct covalent post-synthetic modification of Cr-MIL-101 using nitrating acid. *Chem. Commun.* **2011**, *47*, 2838-2840.

32) Lun, D. J. Waterhouse, G. I. N.; Telfer, S. G. A General Thermolabile Protecting Group Strategy for Organocatalytic Metal—Organic Frameworks. *J. Am. Chem. Soc.* **2011**, *133*, 5806-5809.

33) Genna, D. T.; Wong-Foy, A. G.; Matzger, A. J.; Sanford, M. S. Heterogenization of Homogeneous Catalysts in Metal Organic Frameworks via Cation Exchange. *J. Am. Chem. Soc.* **2013**, *135*, 10586-10589.

34) Das, S.; Kim, H.; Kim, K. Metathesis in Single Crystal: Complete and Reversible Exchange of Metal Ions Constituting the Frameworks of Metal—Organic Frameworks. *J. Am. Chem. Soc.* **2009**, *131*, 3814-3815.

35) Burnett, B. J.; Barron, P. M.; Hu, C.; Choe, W. Stepwise Synthesis of Metal—Organic Frameworks: Replacement of Structural Organic Linkers. *J. Am. Chem. Soc.* **2011**, *133*, 9984-9987.

36) Kim, M.; Cahill, J. F.; Su, Y.; Prather, K. A.; Cohen, S. M. Postsynthetic ligand exchange as a route to functionalization of 'inert' metal—organic frameworks. *Chem. Sci.* **2012**, *3*, 126-130.

37) Karagiaridi, O.; Bury, W.; Sarjeant, A. A.; Stern, C. L.; Farha, O. K.; Hupp, J. T. Synthesis and characterization of isostructural cadmium zeolitic imidazolate frameworks via solvent-assisted linker exchange. *Chem. Sci.* **2012**, *13*, 3256-3260.

38) Xu, Y.; Vermeulen, N. A.; Liu, Y.; Hupp, J. T.; Farha, O. K. SALE-Ing a MOF-Based "Ship of Theseus." Sequential Building-Block Replacement for Complete Reformulation of a Pillared-Paddlewheel Metal—Organic Framework. *Eur. J. Inorg. Chem.* **2016**, 4345-4348.

39) Li, T.; Kozlowski, M. T.; Doud, E. A.; Blakely, M. N.; Rosi, N. L. Stepwise Ligand Exchange for the Preparation of a Family of Mesoporous MOFs. *J. Am. Chem. Soc.* **2013**, *135*, 11688-11691.

40) Kang, Z.; Fan, L.; Sun, D. Recent advances and challenges of metal—organic framework membranes for gas separation. *J. Mater. Chem. A*. **2017**, *5*, 10073-10091.

41) Li, J.-R.; Sculley, J.; Zhou, H.-C. Metal—Organic Frameworks for Separations. *Chem. Rev.* **2012**, *112*, 869-932.

42) Luna-Triguero, A.; Vincent-Luna, J. M.; Gomez-Alvarez, P.; Calero, S. Olefin/Paraffin Separation in Open Metal Site Cu-BTC Metal—Organic Framework. *J. Phys. Chem. C* **2017**, *121*, 3126-3132.

43) Murray, L. J.; Dinca, M.; Yano, J.; Chavan, S.; Bordiga, S.; Brown, C. M.; Long, J. R. Highly-Selective and Reversible O2 Binding in Cr3(1,3,5-benzenetricarboxylate)2. *J. Am. Chem. Soc.* **2010**, *132*, 7856-7857.

44) Kizzie, A. C.; Wong-Foy, A. G.; Matzger, A. J. Effect of Humidity on the Performance of Microporous Coordination Polymers as Adsorbents for CO2 Capture. *Langmuir* **2011**, *27*, 6368-6373.

45) Caskey, S. R.; Wong-Foy, A. G.; Matzger, A. J. Dramatic Tuning of Carbon Dioxide Uptake via Metal Substitution in a Coordination Polymer with Cylindrical Pores. *J. Am. Chem. Soc.* **2008**, *130*, 10870-10781.

46) McDonald, T. M.; Mason, J. A.; Kong, X.; Bloch, E. D.; Gygi, D.; Dani, A.; Crocella, V.; Giordanino, F.; Odoh, S. O.; Drisdell, W. S.; Vlaisavljevich, B.; Dzubak, A. L.; Poloni, R.; Schnell, S. K.; Planas, N.; Lee, K.; Pascal, T.; Wan, L. F.; Prendergast, D.; Neaton, J. B.; Smit, D.; Kortright, J. B.; Gagliardi, L.; Bordiga, S.; Reimer, J. A.; Long, J. R. Cooperative insertion of CO2 in diamine-appended metal—organic frameworks. *Nature* **2015**, *519*, 303-308.

47) Henke, S.; Wieland, D. C. F.; Meilikhov, M.; Paulus, M.; Sternemann, C.; Yusenko, K.; Fischer, R. A. Multiple phase-transitions upon selective CO2 adsorption in an alkyl ether functionalized metal—organic framework—an in situ X-ray diffraction study. *Cryst. Eng. Comm.* **2011**, *13*, 6399-6404.

48) El Osta, R.; Carlin-Sinclair, A.; Guillou, N.; Walton, R. I.; Vermoortele, F.; Maes, M.; de Vos, D.; Millange, F. Liquid-Phase Adsorption and Separation of Xylene Isomers by the Flexible Porous Metal—Organic Framework MIL-53(Fe). *Chem. Mater.* **2012**, *24*, 2781-2791.

49) Padmanaban, M.; Muller, P.; Lieder, C.; Gedrich, K.; Grunker, R.; Bon, V.; Senkovska, I.; Baumgartner, S.; Opelt, S.; Paasch, S.; Brunner, E.; Glorius, F.; Klemm, E.; Kaskel, S. Application of a chiral metal—organic framework in enantioselective separation. *Chem. Commun.* **2011**, *47*, 12089-12091.

Chapter 2

Purification of Chloromethane by Selective Adsorption of Dimethyl Ether on Microporous Coordination Polymers[†]

2.1 Introduction

Chloromethane (MeCl, methyl chloride) is produced on a scale of 650,000 tons per year in the US and is a feedstock for industrial processes; though its primary use is for the synthesis of silicones, it also finds applications in Friedel-Crafts alkylations for the production of alkylbenzenes.[1,2] Oxygenated impurities can lead to significant decreases in process efficiency due to catalyst degradation or side product formation. Industrially, MeCl is synthesized at elevated temperature and pressure by reacting methanol with hydrogen chloride yielding water as a by-product.[3] Dimethyl ether (DME) and hydrochloric acid, side products of the process, are formed by the reaction of MeCl with residual methanol (Figure 2.1). Whereas residual hydrochloric acid, methanol, and water can be simply removed by fractional distillation, DME is more difficult to separate as it shares a boiling point of -24 °C with MeCl. Although the hydrochlorination process above has been optimized such that the amount of DME formed by the side reaction is on the order of 1% of the product stream before purification, this amount is still high enough to cause issues with subsequent reactions of MeCl.[3] In order to further purify MeCl, a chemical method was developed that takes advantage of the reactivity differences between the two molecules. The crude MeCl stream is passed through a column of >78% sulfuric acid in order to convert DME into easily removable methyl sulfate and onium salts, as well as to remove residual water, methanol, and hydrochloric acid.[1] While this process is efficient in purifying the desired MeCl, the amount and toxic nature of the waste streams that are generated in addition to the need for further processing of these waste materials is problematic. The spent sulfuric acid must be purified and further treated if it is to be reused or disposed. With distillation ruled out as an alternative, there have been attempts to separate DME from MeCl using adsorption. Porous

[†] Published: Boissonnault, J. A., Wong-Foy, A. G.; Matzger, A. J. *Langmuir* **2016**, *32*, 9743-9747.

silica and alumina have both been examined for use in the separation and the adsorptive process is reported to yield MeCl at a purity comparable with the reactive purification process.[4,5] To the best of our knowledge, despite the high purity that can be obtained, sorptive separation has not been employed in the purification of industrial process streams of MeCl. Herein we demonstrate the potential of a new class of sorbents to solve this old problem in separations.

Crystalline microporous coordination polymers (MCPs, also known as metal-organic frameworks) are a class of materials composed of metal clusters bridged by polytopic organic linkers to form a 2D or 3D network with regular order. These materials have been explored for a wide range of applications from catalysis to gas storage and separations due to their high porosity and chemical tunability.[6-9] On the separations front, MCPs have previously been shown to separate carbon dioxide from a flue gas stream, to remove water from air, olefins from paraffins, and branched alkanes from linear alkanes.[8,10,11] For the most part, these separations rely on chemical interactions between an analyte in a mixture and the MCP through interactions with the metal clusters and/or the organic linkers though some separations have been reported, at least in part, due to size exclusion.[11] The advantages for MCPs with regards to separations are 1) the high capacity of these materials allowing a significant volume of a mixture to be separated relative to the amount of MCP used and 2) the relative ease of regeneration after adsorption. However, all of the aforementioned separations can also be accomplished using distillation which poses a competing technology as the boiling point differences among the above mixtures are sufficient for modern physical separation techniques.

DME and MeCl present a significant challenge for traditional separations. Their boiling points are -24.8 °C and -24.2 °C, respectively; their molecular weights are 46.07 g/mol and 50.49 g/mol, respectively; and their kinetic diameters are likewise similar. However, based on the chemical differences between DME and MeCl, it is reasonable to propose that MCPs with coordinatively unsaturated metals should prove useful in this separation. Coordinatively unsaturated metal sites arise in MCPs when a solvent molecule from the synthesis (typically water or N,N-dimethyl formamide) bound to the metal cluster is removed using a combination of elevated temperature and vacuum. This changes the coordination number of the metal from typically 6 to 5 while maintaining the coordination geometry allowing for guest molecules to interact with the metal. These coordinatively unsaturated metals are expected to prefer

coordination to the oxygen atom of DME rather than the chlorine atom of MeCl. To test this notion, three MCPs were selected that have coordinatively unsaturated metal sites lining the pores: HKUST-1 has copper(II) paddlewheels, Co/DOBDC has infinite chains of cobalt(II) atoms bridged by carboxylates and phenolates, and MIL-100(Fe) has trinuclear iron(III) clusters, shown in Figure 2.2.[12-14] These MCPs have varying proportions of coordinatively unsaturated metals in their pores with metal densities of 4.90 mmol/g (4.34 mmol/cm^3) for HKUST-1, 6.33 mmol/g (7.44 mmol/cm^3) for Co/DOBDC, and 4.96 mmol/g (3.57 mmol/cm^3) for MIL-100(Fe). In addition to all MCPs here possessing high surface areas (>1300 m^2/g), HKUST-1 and MIL-100(Fe) are produced commercially by the company BASF, as Basolite® C300 and F300 respectively, pointing to potential for large scale deployment. MOF-5 was also examined as a benchmark for the separation in unfunctionalized MCPs as it has traditionally been viewed as a material that lacks high affinity binding sites at the tetranuclear zinc cluster.*

2.2 Results and Discussion

A representative gas mixture of 2% DME in MeCl was flowed over a column containing the adsorbents and the effluent measured using mass spectrometry to determine the gaseous composition (see 2.4 Experimental Methods). As a benchmark of conventional sorbents that have been used for the purification of MeCl, experiments were also conducted using silica gel and alumina. Two different types of silica gel were used with varying pore sizes denoted as grades 635 and 923 with 60 Å and 30 Å pores, respectively. Alumina and silica gels 635 and 923 gave a total DME uptake of 1.03 ± 0.04 wt%, 5.34 ± 0.04 wt% and 5.75 ± 0.04 wt%, respectively. MOF-5 showed a comparable total DME uptake with 2.96 ± 0.08 wt% of DME adsorbed. The low capacity for DME in MOF-5 is likely due to the absence of specific coordination sites for DME to adsorb to in the MCP such that it must compete with MeCl in physisorption. By comparison, MIL-100(Fe) gave a total DME sorption of 8.4 ± 0.1 wt%, HKUST-1 gave 16.9 ± 0.7 wt% and Co/DOBDC gave 25.4 ± 0.5 wt%. Of the MCPs tested, the three with coordinatively unsaturated metal sites had significantly higher capacity than any of the three

*Recent evidence has suggested that the coordination of solvent or other ligands to the zinc centers in MOF-5 is possible. Additional ligands can be accommodated through shifting of the cluster and changing of the coordination environment of one of the four zinc atoms from tetrahedral to octahedral. See, for example: Brozek, C. K.; Michaelis, V. K.; Ong, T.-C.; Bellarosa, L.; López, N.; Griffin, R. G.; Dincă, M. Dynamic DMF Binding in MOF-5 Enables the Formation of Metastable Cobalt-Substituted MOF-5 Analogues. *ACS Cent. Sci.* **2015**, *1*, 252-260.

standard sorbents.

We hypothesized that the selectivity for the sorption of DME compared to MeCl arises directly from the coordinatively unsaturated metal sites. Consequently, MOF-5 which lacks coordinatively unsaturated metal sites shows poor sorption of DME. The high sorption of DME can thus be attributed to the presence of coordinatively unsaturated sites in HKUST-1, Co/DOBDC and MIL-100(Fe). The amount that each coordinatively unsaturated MCP was able to adsorb appears to be directly related to the amount of metal sites that are present in the materials. In this case, Co/DOBDC had the highest amount of adsorbed DME followed by HKUST-1 and MIL-100(Fe). The relatively poor performance of MIL-100(Fe) as compared with HKUST-1, which contains a similar proportion of coordinatively unsaturated metal centers, can be attributed to the presence of fluoride ions that are bound to some of the Fe(III) sites in MIL-100(Fe); this effectively blocks those sites from contributing to adsorption of DME effectively reducing the density of metal centers available for DME binding.[13]

Space velocities are used in flow processes to determine the amount of feedstock that can be processed in an hour over a solid bed. This metric has been used for the efficiency of catalysts as a function of the bed size and the flow rate of the gas as well as in adsorptive separation processes.[16-18] In applying this to the separation of DME from MeCl, the MCPs performed the separations with space velocities on the order of 10,000 h^{-1} at room temperature compared to examples of the sulfuric acid column stream having space velocities on the order of 100 h^{-1}. The separation with MCPs would be able to process 100 times more volume of gaseous mixture than the sulfuric acid column of the same length.[19] During the course of the breakthrough experiment, the front of the DME as it was being adsorbed into the coordinatively unsaturated MCPs could be observed visibly as a color change of the material, ie. HKUST-1 showed a change from a dark, royal blue to a lighter, sky blue hue as the material became saturated with DME (Figure 2.3) and this provides simple monitoring of the breakthrough process as well as regeneration (*vide infra*).

Breakthrough capacity, measured as the amount of guest sorbed to the material before it is detected as exiting the column, was also examined in part to determine how much pure MeCl can be recovered before the materials need to be regenerated. For both silica gels, the breakthrough capacities are nearly ideal in that they are close to the total capacities (Figure 2.4).

Grade 635 was observed to have a breakthrough capacity of 5.17 ± 0.06 wt% and grade 923 had 5.3 ± 0.3 wt%. These resulted in 1.1 L pure MeCl per gram sorbent for each. Alumina, however, showed a negligible breakthrough capacity as DME was immediately detectable, resulting in no pure MeCl from the effluent of the column. This is likely due to the lower affinity of DME for alumina compared to silica gel.

The MCPs had varying results for breakthrough capacity. MOF-5 showed negligible breakthrough capacity for DME similar to alumina. This is consistent with the notion that coordinatively unsaturated sites are required to impart selectivity and that high surface area alone is not adequate. MIL-100(Fe) and HKUST-1 had slightly higher breakthrough capacities than silica gel with 6.4 ± 0.2 wt% and 10 ± 2 wt%, respectively. Co/DOBDC was the only MCP with a significantly higher breakthrough capacity compared to the conventional sorbents showing 16 ± 2 wt%. Due to these higher breakthrough capacities, each of the MCPs with coordinatively unsaturated sites was able to provide significant amounts of pure MeCl from mixed streams. MIL-100(Fe), HKUST-1 and Co/DOBDC produced pure streams of MeCl that amounted to 1.2 L/g, 2.1 L/g and 3.4 L/g, respectively. While MIL-100(Fe) performed similarly to silica gel in this respect, HKUST-1 and Co/DOBDC showed vast improvements in the amount of pure MeCl that could be obtained from the sorptive process. It should be noted based on the total capacity of the MCP sorbents that additional improvements in breakthrough should be achievable with optimization of particle size and bed packing as these factors can have significant impact on breakthrough.

Co/DOBDC was further examined for regenerability after DME uptake as it was the best performing material and has been shown previously to be amenable to sorption under humid environments.[12] After being subjected to the 2% DME in MeCl stream as above, Co/DOBDC was heated to 145 °C under nitrogen flowing at 20 sccm. Effluent from the MCP was monitored by mass spectrometry confirming the removal of DME was complete within 1 hour. Co/DOBDC was recycled in this manner for 10 regeneration cycles and it maintained a total DME capacity of ~22 wt% (Figure 2.5). Not only was Co/DOBDC able to be regenerated, it maintained its heightened capacity for DME over other sorbents. However, the breakthrough capacity of the material suffers over the course of the separation/regeneration process dropping to ~8 wt%. This result does not indicate framework degradation as both the total and the breakthrough capacities

remain relatively constant after an initial decrease. It is more consistent with packing issues of the material in the column that, upon heating, may result in the formation of channels through the material which would lower the breakthrough capacity while maintaining a similar total capacity. Co/DOBDC is able to demonstrate a significant regenerable capacity for DME and provide a larger quantity of pure MeCl than any other sorbent tested.

2.3 Conclusion

MCPs show great potential for the purification of MeCl by sorption of DME as a replacement for current purification methods. The three MCPs tested possessing coordinatively unsaturated metal centers were able to remove a significant quantity of DME diluted in a stream of MeCl largely due to the coordinatively unsaturated metal centers that selectively bind to DME. Among these MCPs, Co/DOBDC had a nearly 5-fold higher total capacity and 3-fold higher breakthrough capacity for DME than silica gel. Additionally, Co/DOBDC was also easily regenerated under mild conditions and still maintained a high total capacity for DME. MCPs are able to provide a significant improvement over previously examined sorptive materials and should provide for a more environmentally and economically efficient purification method than the currently utilized sulfuric acid scrubbing.

2.4 Experimental Methods

Materials: Methyl chloride (99.9%) and dimethyl ether (99.5%) were purchased from Cryogenic Gases. All materials and instrumentation used in the breakthrough experiment with MeCl involved were carefully chosen to exclude any brass or aluminum components as MeCl is known to react with aluminum and zinc to form pyrophoric methyl aluminum and methyl zinc. Davisil grades 923 and 635 were purchased from Sigma Aldrich and were heated at 150 °C under dynamic vacuum for 24 hours prior to use. Activated alumina (50-200 μm) was purchased from Acros Organics and used as obtained. The MCPs HKUST-1, MIL-100(Fe), Co/DOBDC and MOF-5 were synthesized and activated according to reported literature procedures.[12-15] Briefly, HKUST-1 was activated at 150 °C under vacuum for 18 hours, MIL-100(Fe) was activated at 150 °C under vacuum for 18 hours, Co/DOBDC was activated at 250 °C under vacuum for 18 hours and MOF-5 was activated at room temperature under vacuum for 18 hours. Upon

activation, MCPs were stored under an inert atmosphere until use. Mass spectrometry experiments were performed using a Hiden Analytical HPR-20 QIC Gas Analysis System.

Breakthrough Experimental: A diagram of the apparatus is shown in Figure 2.10. Sorbent material (~30mg) prepared above was loaded into a glass tube (O.D. 1/4", I.D. 0.148") supported by glass wool on either end under an inert atmosphere. The tube (1) was placed in line with the flow system under a flow of nitrogen gas. Chloromethane (49 sccm, 2) and dimethyl ether (1 sccm, 3) gases were mixed in line prior to flow over the sorbent. The flow rate of the gas mixture was adjusted to 10 sccm using an MFC and back-pressure valve (4) before flowing through the sorbent. The effluent from the system was measured through a residual gas analyzer (5) mass spectrometer observing peaks at 28, 46 and 51 mass units to observe dinitrogen, DME and MeCl respectively.

The switch at (6) allowed for the sorbent packed into a glass tube to be kept under nitrogen flow until the experiment was started by flipping the switch to the MeCl/DME mixture. Due to this, there is a dead volume in the system corresponding to the volume that the gas mixture has to fill before it can be seen by the detector. The dead volume of the system was calculated by switching the gas mixture with a column packed with an amount of glass wool similar to that used to hold MCP and measuring the amount of time it took for MeCl/DME to be detectable by the mass spectrometer. This gave a calculated dead volume of 2.21 ± 0.05 mL which is further subtracted from all of the results as described below.

Mass spectrometry data are collected at a rate of 3 Hz with the components given as a partial pressure (Torr). Breakthrough experiments were allowed to proceed until the mixture had achieved equilibrium for both gases.

The data is converted to volume of gas by first determining a flow factor that corresponds to the signal of the gas at the maximum in the flow system (ie. 98% for MeCl and 2% for DME). The flow factor is determined by:

$$ff_{gas} = \frac{flow\ rate_{gas}}{s_{eq}}$$

where *ff* is the flow factor in mL/(s·torr), flow rate is given as mL/s for that gas as a part of the mixture, and s_{eq} is the signal of the gas at equilibrium given in torr. From this, the volumetric

flow rate can be determined by multiplying *ff* by the signal at each time point. This can then be used to determine the volume of gas that has flowed into the system over each separate time point A and A-1 using the trapezoidal approximation:

$$Vol_A = \left(ff * (s_A + s_{A-1})\right) * 0.5 * (t_A - t_{A-1})$$

where s_A is the signal at time point A, $s_{A\text{-}1}$ is the signal of the time point directly before time point A, and t_A and $t_{A\text{-}1}$ are those respective times in seconds. The total capacity of gas adsorbed by the sorbent in each run is given by the theoretical amount of gas flowed over the system less the dead volume of the system and the sum of the gas detected at each point calculated as above:

$$Vol_{total} = flow\ rate * t_{eq} - Dead\ Volume - \sum_{A}^{teq} Vol_A$$

with t_{eq} being the time until equilibrium is reached. Each volume adsorbed was averaged across three separate runs for each material.

Volume of pure MeCl obtained from each sample is determined by calculating the amount of MeCl detected before the appearance of DME in the mass spectrometer. This is done by subtracting the amount of MeCl adsorbed to the MCP from the total amount of MeCl that flows through the system before detection of DME as:

$$Pure\ MeCl = flow\ rate * t_{DME,bkth} - Dead\ Volume - \sum_{A}^{t_{MeCl,eq}} Vol_{MeCl,A}$$

where t_{bkth} is the time of breakthrough of the gas component when it is detected by the mass spectrometer. The volume of pure MeCl is calculated separately for each run and averaged for each material.

Regeneration of Co/DOBDC: A sample Co/DOBDC subjected to the above gas mixture stream was regenerated in its glass column on the system using a heating jacket. The material was heated to an internal temperature of 145 °C under nitrogen flowing at a continual rate of 20 sccm. The effluent was monitored by RGA mass spectrometry and the sample was heated until no more DME was observed. The column was then allowed to cool under flowing nitrogen until it reached ambient temperature. The material was then subjected to the MeCl/DME stream as

above to determine any differences in the separation properties. Regeneration cycles were monitored by the mass spectrometer at a rate of 0.3 Hz.

2.5 Figures

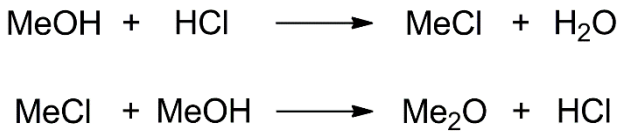

Figure 2.1. Reaction schemes for the formation of dimethyl ether from methanol and hydrogen chloride and for the side reaction of methyl chloride with methanol to form dimethyl ether and hydrochloric acid. The reaction industrially is conducted at elevated temperature and pressure in batch.

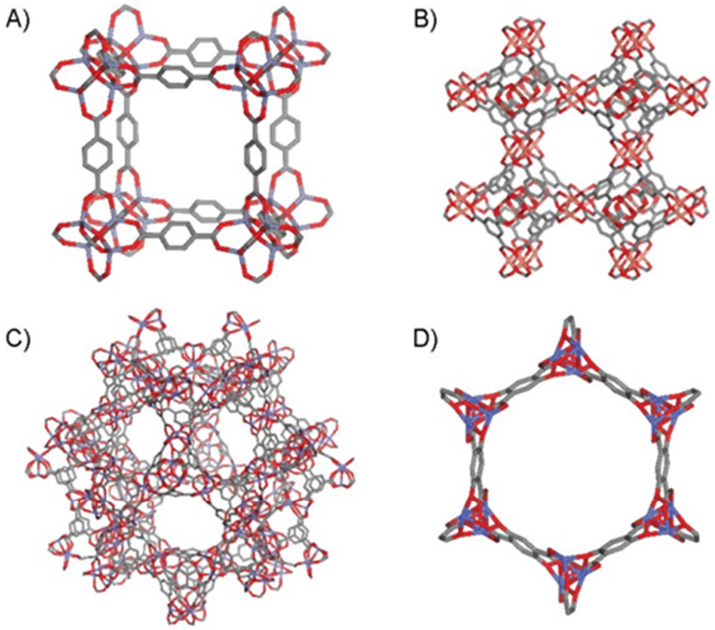

Figure 2.2. Structures of the MCPs employed herein for MeCl/DME separation: A) MOF-5 (Zn_4O(terephthalate)$_3$; B) HKUST-1 (Cu_3(trimesate)$_2$; C) MIL-100(Fe) (Fe_3O(trimesate)$_2$); D) Co/DOBDC (Co_2(2,5-dioxidoterephthalate), MOF-74-Co, CPO-27-Co).

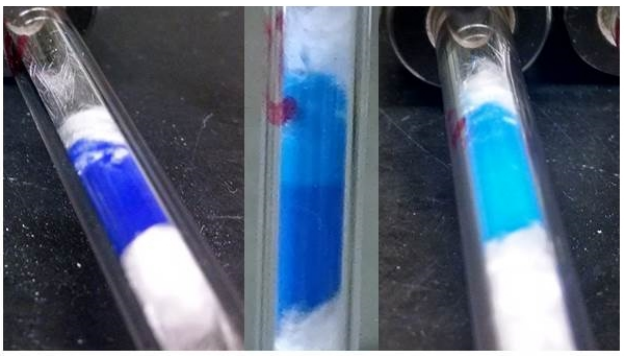

Figure 2.3. Packed columns of HKUST-1 and the observed color change of the material from before (left), during (middle), and after (right) sorption of DME via flowing a 2% DME in MeCl mixture.

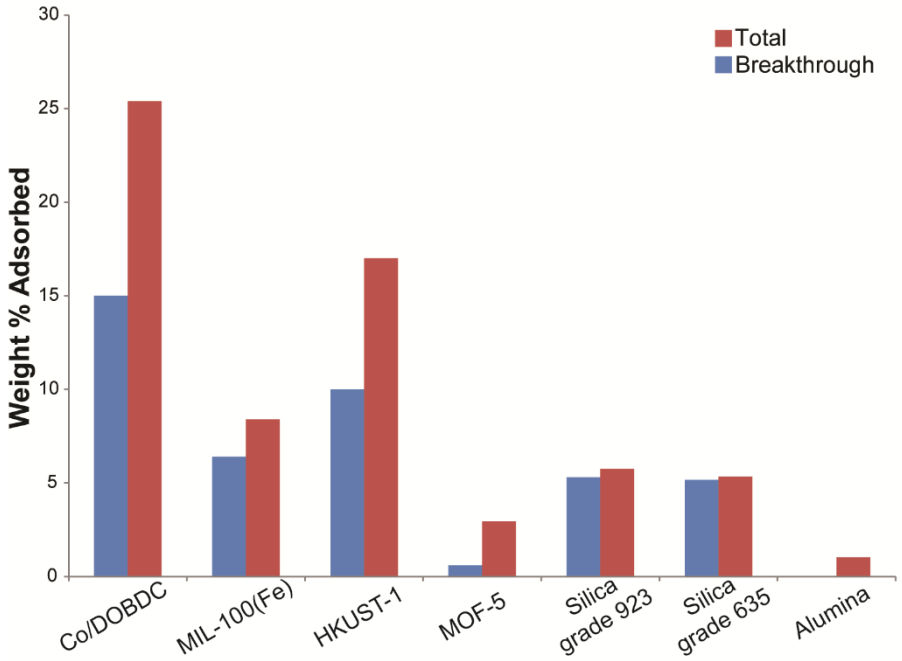

Figure 2.4. Comparison of DME sorption capacities at breakthrough and at equilibrium for MCPs and conventional sorbents under flow through conditions.

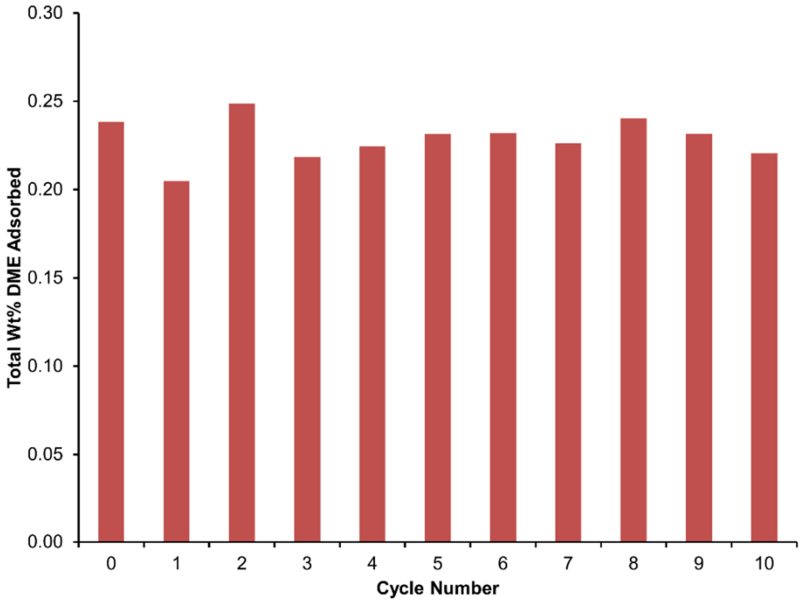

Figure 2.5. Representative regeneration of Co/DOBDC showing total DME capacity over 10 cycles. Co/DOBDC was regenerated after each cycle by flowing N_2 through the column and heating to 145 °C.

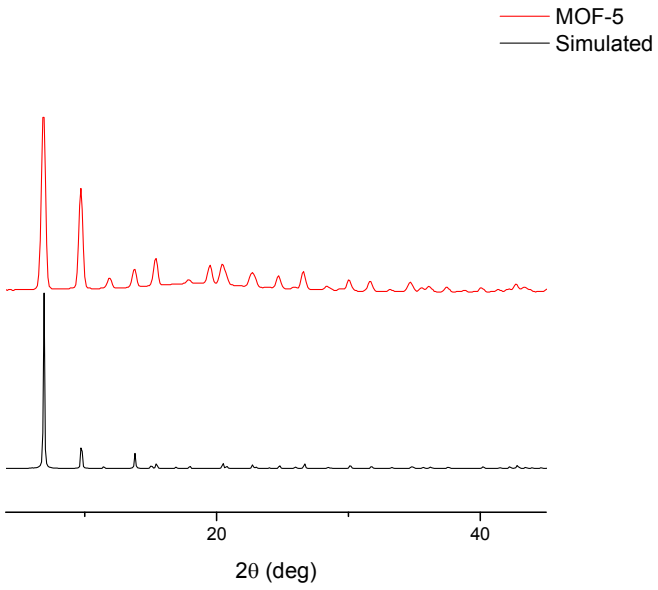

Figure 2.6. PXRD pattern of as-synthesized MOF-5 compared to the pattern simulated from the crystal structure.

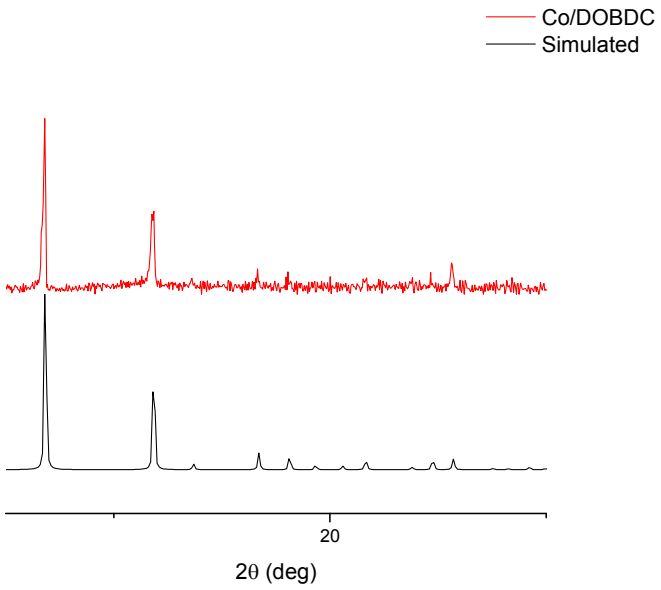

Figure 2.7. PXRD pattern of as-synthesized Co/DOBDC compared to the pattern simulated from the crystal structure.

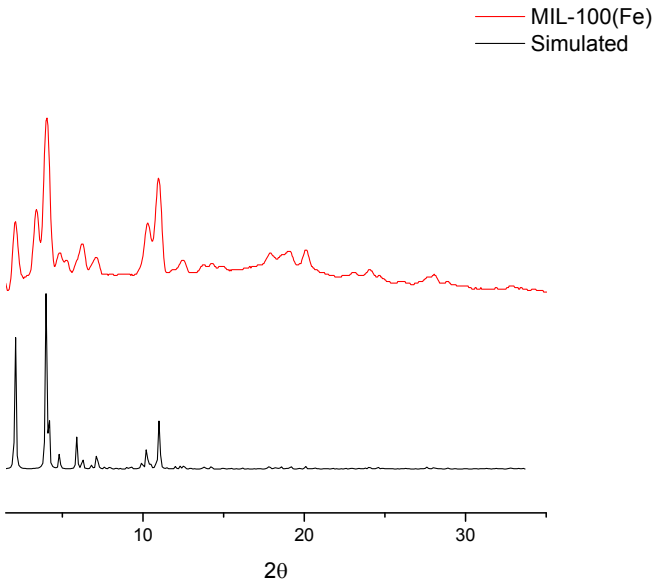

Figure 2.8. PXRD pattern of as-synthesized MIL-100(Fe) compared to the pattern simulated from the crystal structure.

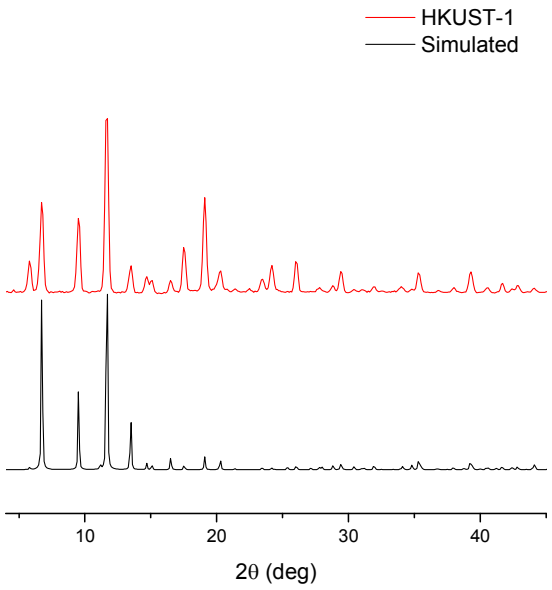

Figure 2.9. PXRD pattern of as-synthesized HKUST-1 compared to the pattern simulated from the crystal structure.

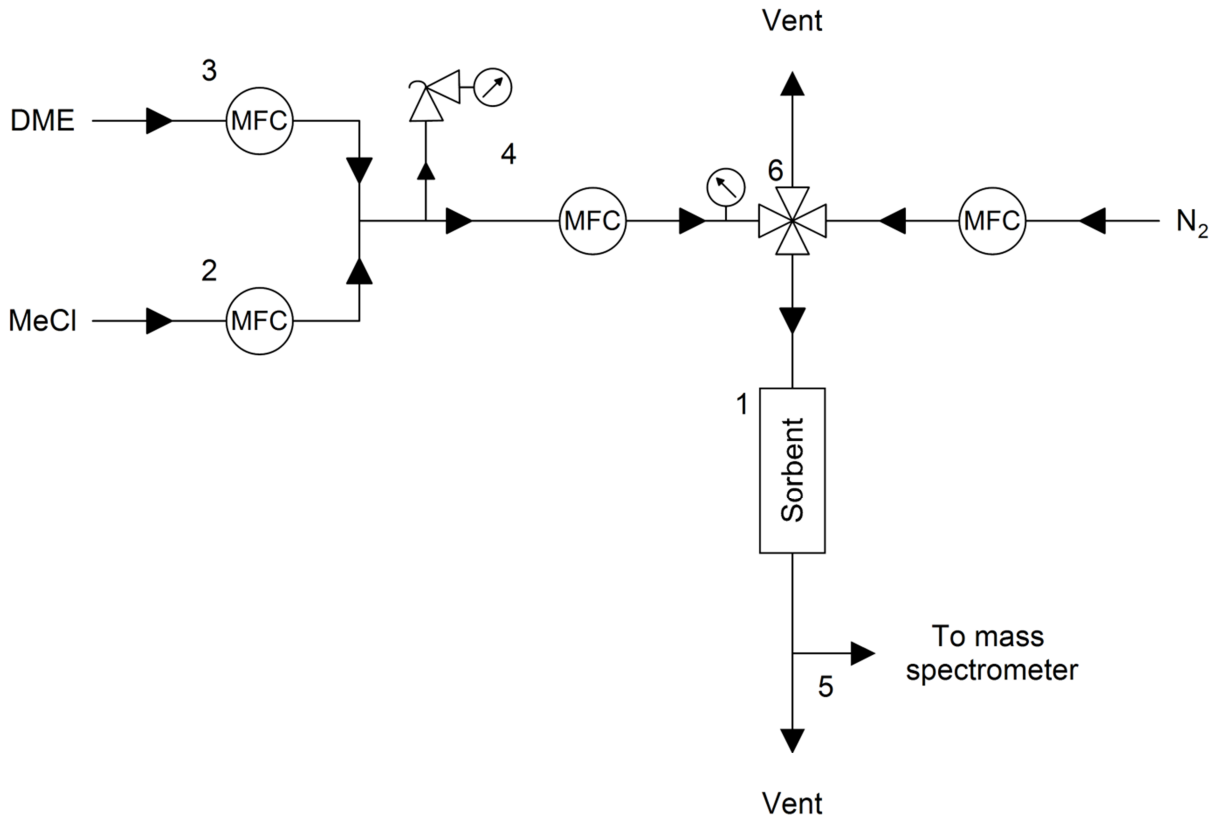

Figure 2.10. Block flow diagram of flow-through apparatus. The sorbent is loaded into a glass column (1). MeCl (2) and DME (3) are mixed at the flow-rates specified above and the total flow rate is stepped down to 10 sccm with excess pressure released from back-pressure regulator (4). The effluent is measured by RGA-MS (5). A four way valve allows for switching between the gaseous mixture and N_2 (6).

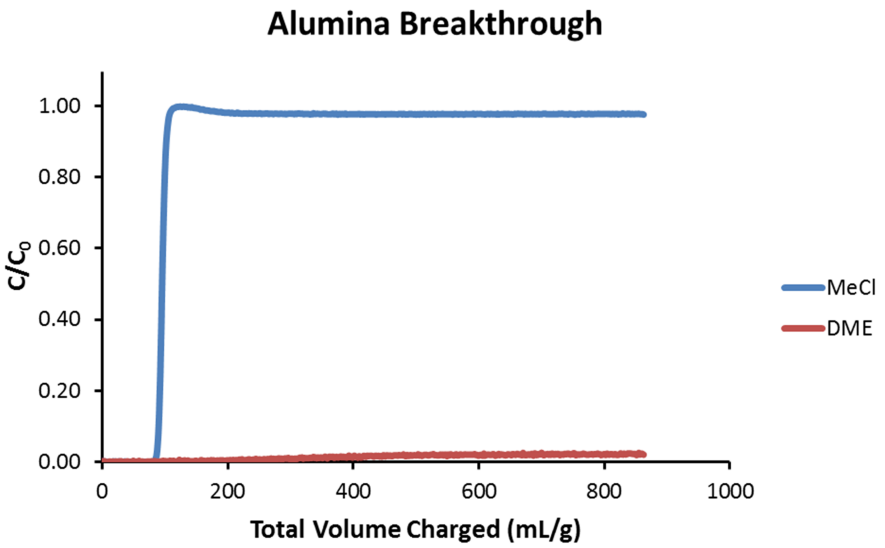

Figure 2.11. DME/MeCl breakthrough curve of activated alumina.

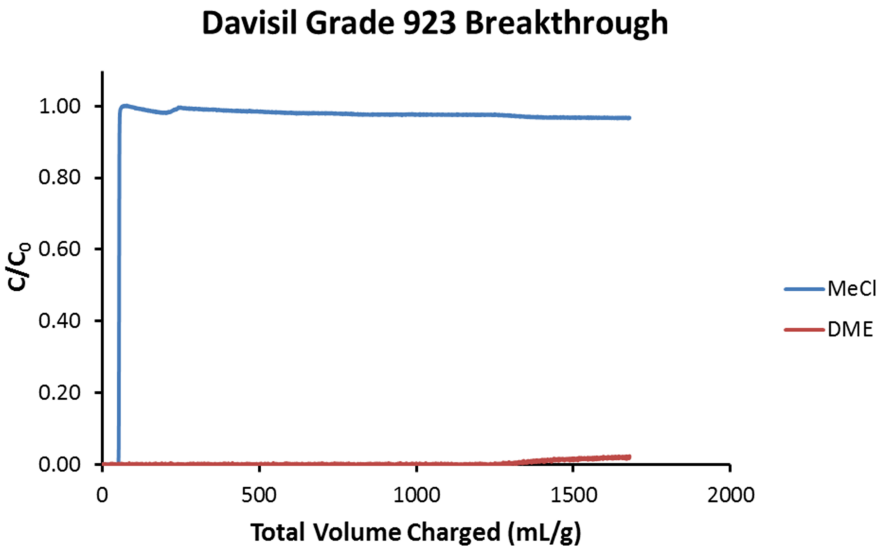

Figure 2.12. DME/MeCl breakthrough curve of Davisil grade 923.

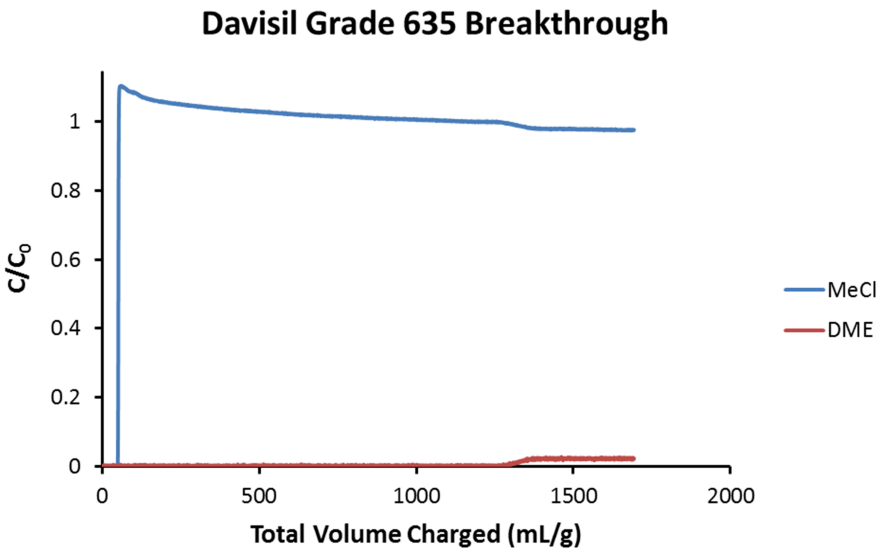

Figure 2.13. DME/MeCl breakthrough curve of Davisil grade 635.

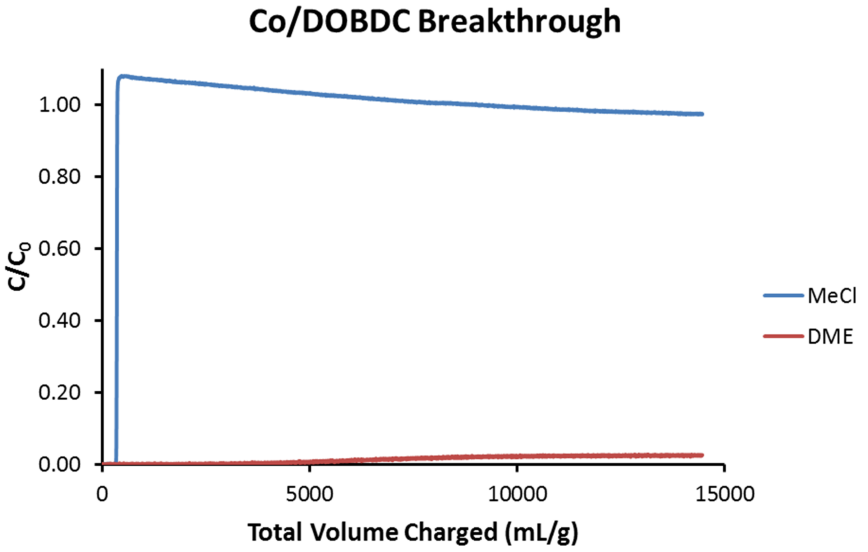

Figure 2.14. DME/MeCl breakthrough curve of Co/DOBDC.

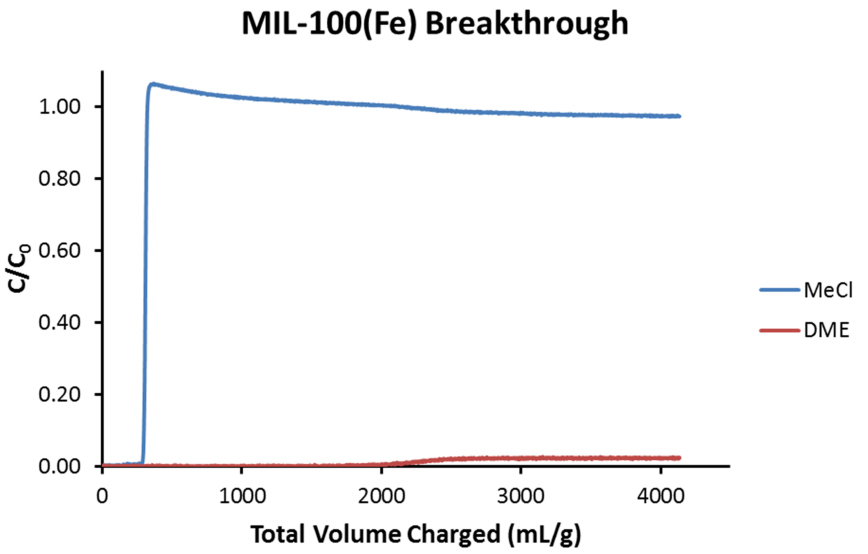

Figure 2.15. DME/MeCl breakthrough curve of MIL-100(Fe).

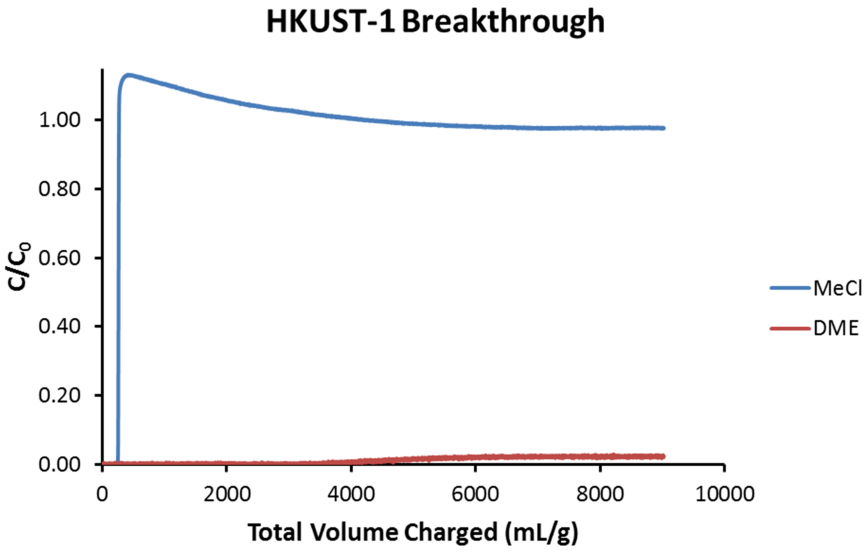

Figure 2.16. DME/MeCl breakthrough curve of HKUST-1.

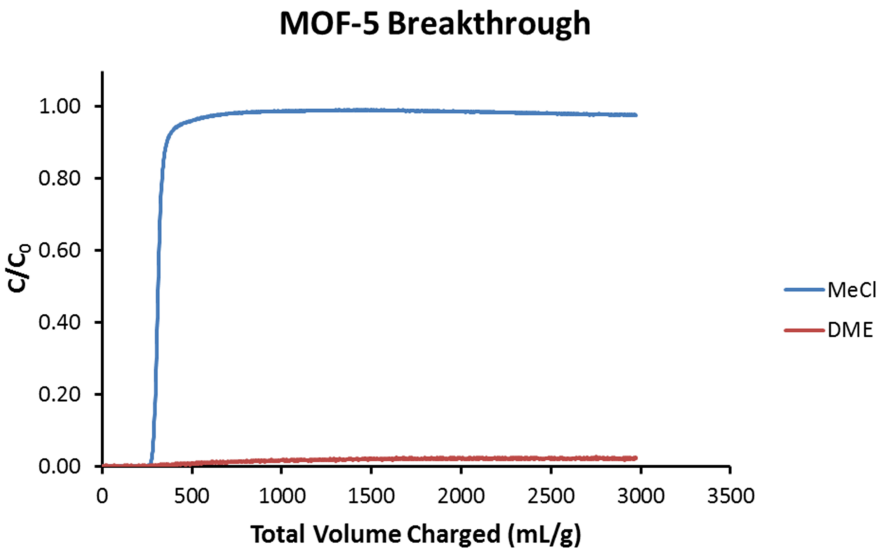

Figure 2.17. DME/MeCl breakthrough curve of MOF-5.

2.6 Tables

Table 2.1. BET surface area calculation of the MCPs used for the breakthrough experiments.

Sample	BET surface area (m^2/g)
MOF-5	**3032**
MIL-100(Fe)	**2176**
HKUST-1	**1188**
Co/DOBDC	**1146**

2.7 References

(1) Chloromethanes. *Ullmann's Encyclopedia of Industrial Chemistry* [online]; Wiley-VCH Verlag GmbH & Co. KGaA, Posted October 15, 2011, http://dx.doi.org/10.1002/14356007.a06_233.pub3 (accessed May 1, 2015).

(2) Lennon, D. P.; Parker, S. F. Inelastic Neutron Scattering Studies of Methyl Chloride Synthesis over Alumina. *Acc. Chem. Res.* **2014**, *47*, 1220-1227.

(3) Crow, R. D.; Roberts N. P. Process for Manufacturing Methyl Chloride. U.S. Patent 6,111,153, 2000.

(4) Yowell, H. L.; Morrell, E.; Morrell, C. M. Purifying Alkyl Halides. U.S. Patent 2,458,819, 1949.

(5) Schneider, O.; Müller, R.; Weissenbach, G. Process for the Purification of Monohalogenoalkanes. European Patent Application 0201738, 1986.

(6) Peng, Y.; Krungleviciute, V.; Eryazici, I.; Hupp, J. T.; Farha, O. K.; Yildirim, T. Methane Storage in Metal-Organic Frameworks: Current Records, Surprise Findings, and Challenges. *J. Am. Chem. Soc.* **2013**, *135*, 11887-11894.

(7) McGuirk, C. M.; Katz, M. J.; Stern, C. L.; Sarjeant, A. A.; Hupp, J. T.; Farha, O. K.; Mirkin, C. A. Turning On Catalysis: Incorporation of a Hydrogen-Bond-Donating Squaramide Moiety into a Zr Metal-Organic Framework. *J. Am. Chem. Soc.* **2015**, *137*, 919-925.

(8) Guo, P.; Wong-Foy, A. G.; Matzger, A. J. Microporous Coordination Polymers as Efficient Sorbents for Air Dehumidification. *Langmuir* **2014**, *30*, 1921-1925.

(9) Genna, D. T.; Wong-Foy, A. G.; Matzger, A. J.; Sanford, M. S. Heterogenization of Homogeneous Catalyst in Metal-Organic Frameworks via Cation Exchange. *J. Am. Chem. Soc.* **2013**, *135*, 10586-10589.

(10) Geier, S. J.; Mason, J. A.; Bloch, E. D.; Queen, W. L.; Hudson, M. R.; Brown, C. M.; Long, J. R. Selective Adsorption of Ethylene Over Ethane and Propylene Over Propane in the Metal-Organic Frameworks M2(dobdc) (M = Mg, Mn, Fe, Co, Ni, Zn). *Chem. Sci.* **2013**, *4*, 2054-2061.

(11) Chen, B.; Liang, C.; Yang, J.; Contreras, D. S.; Clancy, Y. L.; Lobkovsky, E. B.; Yaghi, O. M.; Dai, S. A Microporous Metal-Organic Framework for Gas-Chromatographic Separation of Alkanes. *Angew. Chem. Int. Ed.* **2006**, *45*, 1390-1393.

(12) Kizzie, A. C.; Wong-Foy, A. G.; Matzger, A. J. Effect of Humidity on the Performance of Microporous Coordination Polymers as Adsorbents for CO2 Capture. *Langmuir* **2011**, *27*, 6368-6373.

(13) Horcajada, P.; Surble, S.; Serre, C.; Hong, D. Y.; Seo, Y. K.; Chang, J. S.; Greneche, J. M.; Margiolaki, I.; Ferey, G. Synthesis and Catalytic Properties of MIL-100(Fe), an Iron(III) Carboxylate with Large Pores. *Chem. Commun.* **2007**, 2820-2822.

(14) Chui, S. S.; Lo, S. M.; Charmant, J. P. H.; Orpen, A. G.; Williams, I. D. A Chemically Functionalizable Nanoporous Material $[Cu_3(TMA)_2(H_2O)_3]_n$. *Science* **1999**, *283*, 1148-1150.

(15) Yaghi, O. M.; Li, H.; Eddaoudi, M.; O'Keeffe, M. Design and Synthesis of an Exceptionally Stable and Highly Porous Metal-Organic Framework. *Nature* **1999**, *402*, 276-279.

(16) Shi, F.; Hammoud, M.; Thompson, L. T. Selective Adsorption of Dibenzothiophene by Functionalized Metal Organic Framework Sorbents. *Appl. Catal. B-Environ.* **2011**, *103*, 261-265.

(17) Cychosz, K. A.; Wong-Foy, A. G.; Matzger, A. J. Enabling Cleaner Fuels: Desulfurization by Adsorption to Microporous Coordination Polymers. *J. Am. Chem. Soc.* **2009**, *131*, 14538-14543.

(18) Fogler, H. S. *Essentials of Chemical Reaction Engineering*; Prentice Hall, Upper Saddle River, NJ, USA 2011.

(19) Edgar, A. T.; Arthur, I. M. Purification of Methyl Chloride. U.S. Patent 2,421,441, 1947.

Chapter 3

Core-Shell Structures Arise Naturally During Ligand Exchange in Metal—Organic Frameworks[†]

3.1 Introduction

Among the host of synthetic strategies for introducing functionality into metal-organic frameworks (MOFs), postsynthetic ligand exchange (PSE or its equivalent solvent-assisted ligand exchange) has enjoyed widespread application due to the operational simplicity and seemingly widespread generality of the approach.[1-4] PSE typically involves incubating crystals of the fully formed framework in a solution of another pure ligand in a suitable solvent such as N,N-dimethylformamide (DMF) or water. The amount of ligand used in PSE reactions varies depending on the desired end product. If complete replacement of a MOF's parent ligands is desired, an excess of ligand (>4 equivalents) is used.[5-7] When a small amount of incorporation is desired (i.e. ligand-bound catalyst), a stoichiometric ratio of 1:1 (ligand:linker) or less is used.[8-11] While PSE has been applied extensively and has shown a large degree of compatibility with ligands of different functionality and various framework types, little is known about the exchange mechanism. This in turn means that the microstructure (linker distribution) within the product is unknown. The microstructure is expected to be rather important for dictating the properties of the material because, for a given composition, linker distribution is expected to change interactions with guests which, in turn, are expected to impact applications.

At the outset of these studies we envisioned two limiting outcomes for the ligand exchange process: core-shell and uniform distribution. These two different architectures can arise due to a number of factors in the ligand exchange process but can be most simply related to the diffusion of the ligand into the pores of the MOF and the rate of the exchange process. If ligand diffusion into the MOF is fast relative to exchange, a uniform and random distribution of substituted linkers is expected. Alternatively if diffusion is very slow or if exchange is much

[†] Published: Boissonnault, J. A.; Wong-Foy, A. G.; Matzger, A. J. *J. Am. Chem. Soc.* **2017**, *139*, 14841-14844.

faster at the edges of the crystal, a limiting, core-shell architecture is expected (Figure 3.1). In cases where ligand size effects disfavor substitution within the material, as recently demonstrated by Rosi and coworkers, the out-come is more likely to involve preferential reaction on the outer surface due to the high enthalpic penalty associated with disrupting the lattice structure in the bulk.[12] Similarly, for cases where there is a strong enthalpic driving force for exchange the microstructural outcome may be skewed.[13] Recently, Ott and coworkers showed that after PSE both exchanged and parent linkers were uniformly dispersed throughout microcrystalline UiO-66 (UiO, University of Oslo) by using Rutherford backscattering spectrometry.[14] However, in this case 2-iodobenzene-1,4-dicarboxylic acid was used as the exchanging ligand despite the effects that iodine may have on the exchange rate (steric or electronic). To explore the process of ligand exchange within MOFs in the absence of enthalpic driving forces, a ligand substitution experiment was designed where the MOF linker would be replaced by its deuterated counterpart, leaving only entropic driving forces for the exchange process.

Herein we propose a new method to examine the microstructure of MOFs after PSE reactions utilizing 2-D mapping Raman microscopy of sectioned crystals. This will allow for an unambiguous image of the distribution of ligands through the material. This meant that the MOFs chosen for this study had to be obtainable as larger single crystals in order to be properly sectioned and allow for them to be mapped. Additionally, MOFs were selected that used benzene-1,4-dicarboxylate (BDC) as the ligand in order to maintain consistency across the systems used. To this end, the three MOF systems selected were MOF-5, UMCM-8 (University of Michigan Crystalline Material), and UiO-66 (University of Oslo) which are described in greater detail below.

3.2 Results and Discussion

MOF-5 was selected as a model system for examining ligand exchange. The structure is composed of tetranuclear basic zinc acetate clusters bridged by BDC yielding a cubic structure with large pores that should allow for facile diffusion of ligands into the MOF during the exchange.[15] Additionally, the large crystal size of MOF-5 (~700-1000 μm) is amenable for analysis of single crystals after the exchange process. 2,3,4,5-Tetradeutero-benzene-1,4-dicarboxylic acid (H_2BDC-d_4) was the ligand selected to be incorporated as it is effectively structurally and chemically identical to H_2BDC. The ligands would however be easily

distinguishable through vibrational spectroscopy due to differences in the stretching and bending frequencies between the C-H and C-D bonds (See Section 3.5). Previous PSE studies with MOF-5 by Gross *et al.* have shown that incorporation of 2-bromoterephthalic acid can be induced at 85 °C in N,N-diethylformamide and water; however, when these conditions were attempted, the resulting exchanged product had fractured from larger single crystals of MOF-5 into smaller crystallites that were not amenable to spatially resolved compositional analysis.[16] To circumvent this, a new method of PSE of single crystals of MOF-5 was developed using dilute solutions of H_2BDC-d_4 in either THF and DMF (0.01M with a ratio of H_2BDC-d_4:BDC = 1:1) at room temperature overnight (18 hours) on a shaker. To ensure the removal of any excess ligand not bound to the MOF, the crystals were exhaustively washed with the selected solvent. The single crystals were then exchanged into CH_2Cl_2, filtered, embedded in an epoxy resin, sectioned on an ultramicrotome, and analyzed by mapping of the sectioned surface with a Raman microscope.

Raman maps of the sectioned crystals after PSE (18 hours) showed the formation of a core-shell architecture where incorporation of BDC-d_4 occurs at the surface and extends inwards towards the center of the crystal with an exchange depth of ~80 μm (Figure 3.2). The shell is still a mixture of both BDC and BDC-d_4 with the highest concentration of deuterated linkers on the surface rapidly decreasing towards the center of the crystal. When the crystals are left to soak for 72 hours in the exchange solution or are heated to 45 °C, the depth of the exchange increases to ~160 μm in both instances but exchange at the core of the MOF was still not observed. Even when the exchange was performed in a saturated solution of H_2BDC-d_4 in THF, exchange at the core of MOF-5 did not occur after heating at 45 °C for 1 week. To increase the concentration of H_2BDC-d_4 in solution, DMF was employed as the exchange solvent. As there is a significant difference in the diffusion coefficient of H_2BDC in DMF and THF (5.43×10^{-10} m^2/s and 10.0×10^{-10} m^2/s respectively), exchange was first conducted at 0.01M H_2BDC-d_4 at room temperature for 18 hours to compare to initial experiments in THF. Raman analysis of sectioned crystals showed a similar core-shell pattern and the depth of exchange was similar to that observed with THF. This indicates that diffusion through the bulk solution is not limiting with respect to the depth of exchange. Increasing the concentration of H_2BDC-d_4 to 0.1M in DMF allowed for exchange at the core of the MOF-5 crystals to be observed after 3 days of incubation while still

maintaining the gradient observed above. It should be noted, however, that at this concentration large cracks had formed throughout the crystals. Powder X-ray diffraction (PXRD) measurements of the crystals after exchange confirmed that, despite the cracking, the structural integrity of MOF-5 was maintained (Figure 3.3). Raman maps of these sectioned crystals suggest that the cracks expedite the incorporation of the ligand into the interior of the crystal by providing a new surface for the ligand to diffuse into the crystal (Figures 3.4 and 3.5). However, the gradient that is observed is consistent with other exchange experiments in DMF and THF implying that diffusion through the bulk of the crystal is ultimately responsible for exchange at the center of the crystal.

To explore the generality of the above observations, UMCM-8 (UMCM, University of Michigan Crystalline Material), was examined due to the increased pore size that may allow for better diffusion into the core of the MOF.[17] UMCM-8 utilizes the same metal cluster as MOF-5; however, by combining H_2BDC and 2,6-naphthalene dicarboxylic acid as co-linkers, a higher porosity, surface area, and pore aperture is achieved while thwarting interpenetration. When exchange reactions are performed using THF and 0.01 M H_2-BDC-d_4 at room temperature for 18 hours as above, the larger crystals were broken down into smaller crystallites that all contained a mixture of BDC and BDC-d_4 when examined by Raman microscopy. Performing the exchange under dilute conditions (0.005 M) for a shorter period of time allowed for the exchange to occur with only minor damage to the crystal consisting of cracking and an increase in opacity of the otherwise clear crystals. This may have resulted from complications arising due to the presence of two different linear dicarboxylates in the structure that may compete for exchange and ultimately allow for the degradation of the crystals. Analysis of sectioned crystals of UMCM-8 post-exchange showed a similar core-shell architecture that had been observed with MOF-5 with a thin layer of ~40 μm after 30 minutes. This suggests that the core-shell architecture resulting from ligand exchange may be general for the basic zinc-acetate cluster.

The nature of the metal cluster dramatically influences PSE rates to the point where each individual system would need to be examined to make conclusions about the micro-structure of the exchange. UiO-66 is a robust MOF composed of the hexanuclear $Zr_6(\mu_3\text{-}O)_4(\mu_3\text{-}OH)_4(CO_2)_{12}$ cluster linked by BDC to form a 3D material.[18] Despite its reported stability, UiO-66 is well-known for being susceptible to ligand exchange even under mild conditions and indeed this was

one of the first MOFs wherein PSE was thoroughly studied providing avenues for synthesis of highly stable, functionalized MOFs.[4] When the typical microcrystalline powder of UiO-66 is subjected to exchange with 10 molar equivalents of H_2BDC-d_4 in water, all particles showed a large degree of exchange by Raman spectroscopy after only 1 hour at 85 °C. However, even though it was possible to observe the presence of both BDC and BDC-d_4 in the particles, the particle size was too small to permit further examination of the exchange as above. In order to examine the distribution of the ligands throughout, larger crystals of UiO-66 are necessary. To this end, single crystals of UiO-66 were grown following literature procedures resulting in crystals with sizes near 100 μm which are large enough to be sectioned after PSE.[19,20] The single crystals were subjected to the same conditions used with the microcrystalline powder and sectioned by hand after exhaustive washing. Raman mapping of the sectioned crystals showed a core-shell architecture with a thin shell of ~10 μm after 1 hour at 85 °C (Figure 3.6). As most UiO-66 is not synthesized as large single crystals, it is important to consider the micro structure of the exchange in the microcrystalline powder. Even though the shell of the single crystal UiO-66 is small (~10 μm), the particle sizes of the microcrystalline UiO-66 is on the order of 1-2 μm. This would likely result in apparent uniform dispersity throughout microcrystalline UiO-66, though the nature of the linkers concentrations may still follow a core-shell pattern as demonstrated for the single crystals. This could also be applied in both cases described above where smaller crystals of MOF-5 and UMCM-8 may result in exchange throughout if the crystal sizes are less than twice the exchange depths reported above.

As exchange does not occur uniformly throughout the MOFs, this precludes a mechanism where diffusion is fast and ligand exchange is unselective. However, in all of the presented examples, the pore sizes of the MOFs are known to be large enough that the diffusion of H_2BDC-d_4 should not be hindered through a size exclusion mechanism. To determine if diffusion of H_2BDC-d_4 into MOF-5 is indeed slow, single crystals of MOF-5 were submerged in a 0.01 M solution of H_2BDC-d_4 in DMF and analyzed by confocal Raman microscopy. This allows for the examination of guests present in the center of the crystal while suppressing signal from the ligand present in solution giving a clear picture of the environment in the center of the crystal. After 18 hours, while a substantial degree of exchange had occurred at the edges of the crystals as above, no H_2BDC-d_4 was observed at the center of the crystal (Figure 3.7). H_2BDC-d_4 was

only observed in the center of the crystal after soaking a MOF-5 crystal in a saturated solution of H_2BDC-d_4 in DMF for >1 hour. This is consistent with slow diffusion of H_2BDC-d_4 into MOF-5 and indicates that diffusion may be limiting to the exchange process. In contrast, diffusion of dimethyl-benzene-1,4-dicarboxylate under the same conditions occurred rapidly (<10 min). This indicates that the size of the H_2BDC-d_4 is not an issue but that the presence of the carboxylic acids hinders diffusion. To test this hypothesis, diffusion of benzoic acid and methyl benzoate was examined in MOF-5. The results of this experiment mirror what was observed above, that is benzoic acid was slow to diffuse to the center of MOF-5 and only was observed at the center after degradation had occurred whereas methyl benzoate diffusion occurred rapidly (<10 min) with no degradation. The above experiments support a picture where the carboxylic acid group is slowing the diffusion of H_2BDC-d_4 into MOF-5, presumably through hydrogen bonding to the metal cluster, resulting in the core-shell architecture observed.

3.3 Conclusion

In conclusion, strong core-shell architectures naturally arise from PSE with MOF-5, UMCM-8, and UiO-66. All three examples showed incorporation of BDC-d_4 first at the surface and then, after additional time, extending in towards the center. This occurs due to the slow diffusion of the carboxylic acid ligand into the pores of the MOF allowing for exchange to occur faster than the diffusion. The perfection of the shells on, at least, the micron level is excellent and exceeds that available from epitaxial overgrowth with the additional advantage that concomitant nucleation and growth of pure phases does not compete with shell formation.[21] The shell structure is absolutely advantageous for concentrating catalytic sites on the outer surfaces of MOF crystals as well as for controlled guest access to the core for selective separations. Other systems are currently being examined to understand the microstructure of PSE in MOFs with different ligand coordination environments and linkers with different topicity.

3.4 Experimental Methods

Materials and Methods: Chemicals were used as purchased without purification unless otherwise noted. 2,3,4,5-Tetradeutero-benzene-1,4-dicarboxylic acid (H_2BDC-d_4) 98% atom D, terephthalic acid (H_2BDC), and 2,6-naphthalenedicarboxylic acid (H_2-NDC) were purchased from Sigma Aldrich. $Zn(NO_3)_2 \cdot 6H_2O$ and N,N-dimethylformamide were purchased from Fisher

Scientific. $ZrCl_4$ (anhydrous) was purchased from Strem Chemicals. $ZrOCl_2 \cdot 8H_2O$ was purchased from Alfa Aesar. N,N-diethylformamide (DEF) was purchased from Acros and purified over activated carbon and passed through a silica gel column before use. Epoxy resin used was Poly/Bed® 812 Resin purchased from Ted Pella Inc. Raman spectroscopy was carried out with a Renishaw inVia Raman Microscope equipped with a Leica microscope, 532 nm laser with 1800 lines/mm grating, 785 nm laser with 1200 lines/mm grating, 65 μm slit, and a Renishaw 588v23 detector. Data analysis was conducted using direct classical least squares (DCLS) in WiRE 4.2 using standards of pure materials. Sectioning of crystals was accomplished on a Leica RM 2165 ultramicrotome.

MOF Synthesis: MOF-5, UMCM-8, UiO-66, and UiO-66 single crystal (UiO-66-sc) were synthesized according to reported literature procedures.[15, 17, 19, 20, 22] MOF-5-*d*, UMCM-8-*d*, and UiO-66-sc-*d* were synthesized by adapting above literature procedures utilizing H_2-BDC-d_4 in place of H_2-BDC. Detailed procedures follow below.

Synthesis of MOF-5. H_2-BDC (66 mg, 0.39 mmol) and $Zn(NO_2)_3 \cdot 6H_2O$ (360 mg, 1.2 mmol) were dissolved in DEF (10 mL) in a 20 mL scintillation vial by sonication. The vial was sealed with a polypropylene cap and heated isothermally in an oven at 100 °C for 24 hours yielding clear, cubic crystals. The mother liquor was decanted and the crystals washed with DMF (3 x 10 mL) and then the solvent exchanged with CH_2Cl_2 (3 x 10 mL).

Synthesis of MOF-5-*d*. H_2-BDC-d_4 (70 mg, 0.39 mmol) and $Zn(NO_2)_3 \cdot 6H_2O$ (360 mg, 1.2 mmol) were dissolved in DEF (10 mL) in a 20 mL scintillation vial by sonication. The vial was sealed with a polypropylene cap and heated isothermally in an oven at 100 °C for 24 hours yielding clear, cubic crystals. The mother liquor was decanted and the crystals washed with DMF (3 x 10 mL) and then the solvent exchanged with CH_2Cl_2 (3 x 10 mL).

Synthesis of UiO-66 (powder). $ZrCl_4$ (125 mg, 0.54 mmol) and H_2-BDC (125 mg, 0.75 mmol) were dissolved in DMF (15 mL) by sonication in a 20 mL scintillation vial. Concentrated HCl (1 mL) was added and the solution was mixed. The vial was capped with a polypropylene cap and heated isothermally in an oven at 85 °C for 18 hours yielding white powder. The solid was

separated by centrifugation and washed with DMF (3 x 10 mL). The solvent was then exchanged with methanol (3 x 10 mL).

Synthesis of UiO-66-sc. $ZrOCl_2 \cdot 8H_2O$ (12 mg, 0.037 mmol) and H_2-BDC (5.2 mg, 0.031 mmol) were separately dissolved in 1 mL DEF each. The two solutions were mixed in a 20 mL scintillation vial followed by the addition of 2 mL of formic acid and then mixed. The vial was then capped with a polypropylene cap and heated isothermally in an oven at 135 °C for two days resulting in clear, octahedral crystals with sizes >100 μm. The mother liquor was decanted and the crystals washed with DMF (3 x 10 mL) and then exchanged with CH_2Cl_2 (3 x 10 mL).

Synthesis of UiO-66-sc-*d*. $ZrOCl_2 \cdot 8H_2O$ (12 mg, 0.037 mmol) and H_2-BDC-d_4 (4.9 mg, 0.029 mmol) were separately dissolved in 1 mL of DEF each. The two solutions were mixed in a 20 mL scintillation vial followed by the addition of 2 mL of formic acid and then mixed. The vial was then capped with a polypropylene cap and heated isothermally in an oven at 135 °C for two days resulting in clear, octahedral crystals with sizes >100 μm. The mother liquor was decanted and the crystals washed with DMF (3 x 10 mL) and then exchanged with CH_2Cl_2 (3 x 10 mL).

Synthesis of UMCM-8. H_2-BDC (13 mg, 0.078 mmol), H_2-NDC (17 mg, 0.078 mmol), and $Zn(NO_3)_2 \cdot 6H_2O$ (142 mg, 0.48 mmol) were dissolved in a 20 mL scintillation vial with 6 mL of DEF via sonication. The vial was then capped with a polypropylene cap and heated isothermally in an oven at 85 °C for 2 days yielding clear, block-shaped crystals. The mother liquor was decanted and the crystals washed with DMF (3 x 10 mL) and then exchanged with CH_2Cl_2 (3 x 10 mL).

Synthesis of UMCM-8-*d*. H_2-BDC-d_4 (13 mg, 0.076 mmol), H_2-NDC (17 mg, 0.078 mmol), and $Zn(NO_3)_2 \cdot 6H_2O$ (142 mg, 0.48 mmol) were dissolved in a 20 mL scintillation vial with 6 mL of DEF via sonication. The vial was then capped with a polypropylene cap and heated isothermally in an oven at 85 °C for 2 days yielding clear, block-shaped crystals. The mother liquor was decanted and the crystals washed with DMF (3 x 10 mL) and then exchanged with CH_2Cl_2 (3 x 10 mL).

Ligand Exchange Reactions: All MOFs were dried under high vacuum prior to use at either room temperature (MOF-5 and UMCM-8) or 150 °C (UiO-66 and UiO-66-sc) for 18 hours.

Ligand exchange reactions were performed on MOF-5, UMCM-8, UiO-66 and UiO-66-sc with H_2BDC-d_4 in solutions of THF or DMF while on a heated shaker plate. At the end of the exchange reactions, the crystals were washed with the solvent of reaction 3 times and then exchanged into CH_2Cl_2.

As an example of the ligand exchange procedure, 5.1 mg of MOF-5 was weighed into a 1 dram vial and 1.9 mL of 0.01 M H_2BDC-d_4 in THF was added. The vial was agitated on a shaker for 18 hours. After this time, the solution was decanted and the crystals were washed with THF (5 x 2 mL) and then exchanged into CH_2Cl_2 (3 x 2 mL). Crystals were then filtered from CH_2Cl_2 and immersed in uncured epoxy. The resin was cured at 60 °C overnight.

Calculated Raman Spectra: Spartan 2014 software suite was used for all calculations. Each molecule was drawn in Spartan and the energies minimized using density functional theory with the B3LYP method and the 6-31G* basis set. Vibrational modes of each molecule were calculated from the energy minimized coordinates using B3LYP with the 6-31G* basis set and offset using a scaling factor of 0.960.[23] The spectra of BDC^{2-} and BDC-d_4^{2-} showed a ring-breathing mode at 1578 cm^{-1} and 1550 cm^{-1} respectively. This corresponds to a difference of 28 cm^{-1}. This is identical to the observed difference of 28 cm^{-1} between MOF-5 and MOF-5-*d* using a785 nm laser as well as being similar to the observed difference of 26 cm^{-1} between UiO-66-sc and UiO-66-sc-*d* using a 532 nm laser.

Experimental Raman Spectra of MOFs: Raman spectra of MOF single crystals were collected from MOF material dried as above. MOF-5, MOF-5-*d*, UMCM-8 and UMCM-8-*d* spectra were collected using a 785 nm laser and UiO-66, UiO-66-sc and UiO-66-sc-*d* spectra were collected using a 532 nm laser.

Powder X-ray Diffraction: Powder X-ray diffraction (PXRD) data were collected at ambient temperature on a PANalytical Empyrean diffractometer in Bragg–Brentano geometry using Cu-Kα radiation (1.54187 Å) operating at 45 kV, 40 mA. The incident beam was equipped with a Bragg-BrentanoHD X-ray optic using fixed slits/soller slits. The detector was a silicon-based linear position sensitive X'Celerator Scientific operating in 1-D scanning mode. Data were collected from 3° to 45° 2θ using a step size of 0.0167° 2θ and a count time of at last 10 s per step.

Raman Mapping Experiments: Single crystals of exchanged MOFs soaking in CH_2Cl_2 were collected by filtration. The crystals were then placed in the bottom of a cylindrical mold and uncured epoxy was added on top of the crystals. The mold was then placed in an oven at 60 °C for 24 hours to allow the resin to cure. Crystals of MOF-5 and UMCM-1 were sectioned using an ultramicrotome at 10 μm increments until the center of the crystal was at the surface of the resin. The sectioned, embedded crystals were mapped on Raman microscope using a 50x objective using a 785 nm laser for MOF-5 and UMCM-8 crystals. For UiO-66, the material was fluorescent using a 785 nm laser and so 532 nm laser was used. This however meant that the epoxy resin could no longer be used as the resin fluoresced with a 532 nm laser. As such, the single crystals were immersed in mineral oil using a razor blade and the 532 nm laser was used for mapping of UiO-66 crystals. Line maps of the crystals were taken through the center of the crystal focusing on the presence of peaks at ~1590 and ~1610 cm^{-1}. DCLS analysis using pure component spectra of the MOFs was performed to determine the presence of each component within each exchanged crystal. Three crystals from each PSE condition were examined. The resultant plot was used to determine the depth of the exchange in each of the mapped crystals where the depth of exchange is defined as the distance from the edge of the crystal to until BDC-d_4 comprises <1% of the total composition rounded to the nearest 10 μm. The exchange depth of the three crystals was averaged for each PSE condition.

Diffusion Experiments: Diffusion coefficient determination by ^{1}H NMR spectroscopy: Diffusion coefficients were calculated using diffusion-ordered spectroscopy. DOSY experiments were conducted on a Varian MR400 spectrometer operating at 400 MHz for ^{1}H at 25 °C with no spinning. Spectra were collected using the DgcsteSL_cc pulse sequence (Vnmrj 4.2) with 8 gradient levels from 0.7552 to 19.32 G/cm. The diffusion delay for both experiments was 200 ms with a gradient length of 2 ms for THF-d_8 and 4 ms for DMF-d_7. Both NMR solutions were 0.01M terephthalic acid in THF-d_8 and DMF-d_7 respectively.

Diffusion in MOF-5: A single crystal of MOF-5 soaked in DMF was placed on a microscope slide with a drop of DMF. A glass coverslip was then placed on top of the crystal, sandwiching it between the glass slide and the coverslip. The initial Raman spectrum of the crystal was taken by focusing on the center of the crystal. The solution containing the analyte (benzoic acid, methyl

benzoate or H_2BDC-d_4) was then placed dropwise at the edge of the coverslip allowing for the solution to be pulled under and contact the MOF. Collection of Raman spectra began 1 minute after the solution contacted the MOF crystal and continued for 18 hours (benzoic acid and H_2BDC-d_4) or until equilibrium was reached (methyl benzoate).

3.5 Figures

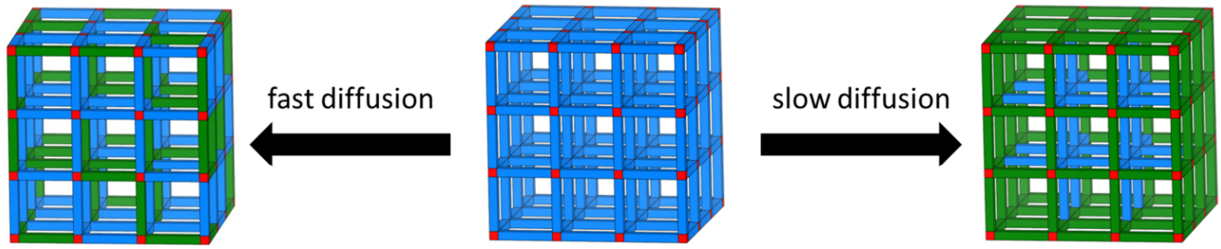

Figure 3.1. Two different ligand incorporation models showing a uniform distribution associated with fast diffusion relative to the exchange process (left) and a core-shell distribution associated with slow diffusion relative to the exchange process.

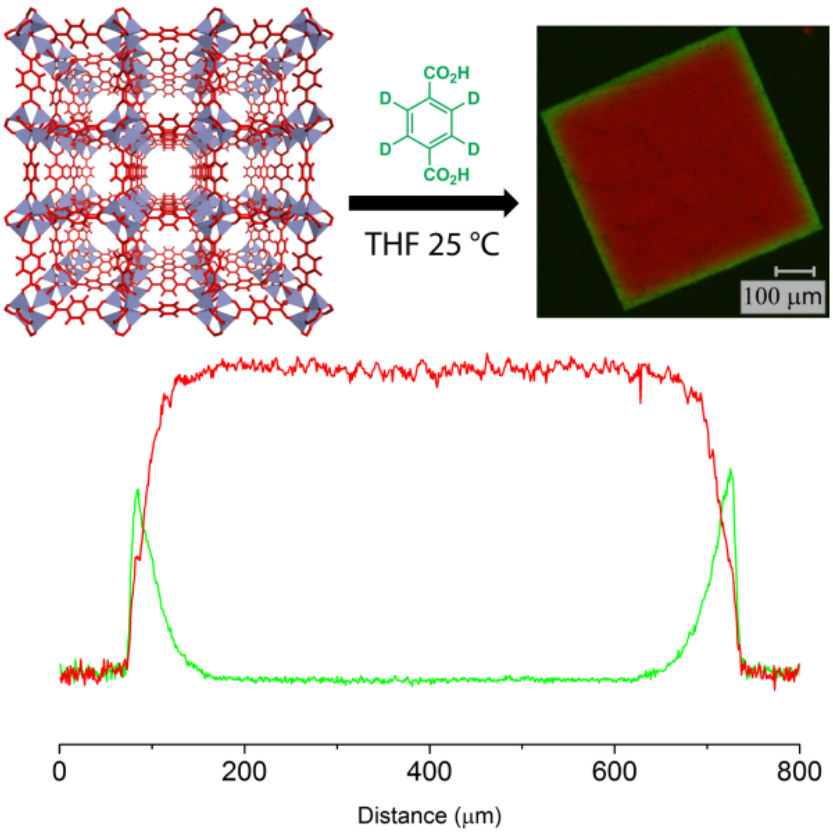

Figure 3.2. Reaction scheme for PSE of MOF-5 with H_2BDC-d_4 (top) yielding a core-shell structure (BDC-d_4–green, BDC–red). A line graph from edge to edge (bottom) shows BDC-d_4 concentrated on the outer edges of the crystal decreasing towards the center.

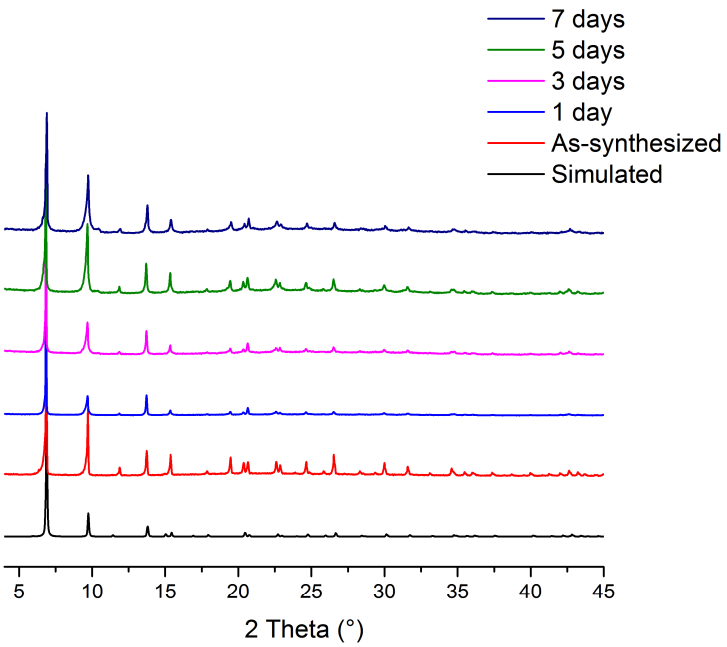

Figure 3.3. Powder X-ray diffraction (PXRD) patterns of MOF-5 after exchange with 0.1 M H_2BDC-d_4 in DMF after 1, 3, 5, and 7 days compared to as synthesized and simulated MOF-5 PXRD patterns.

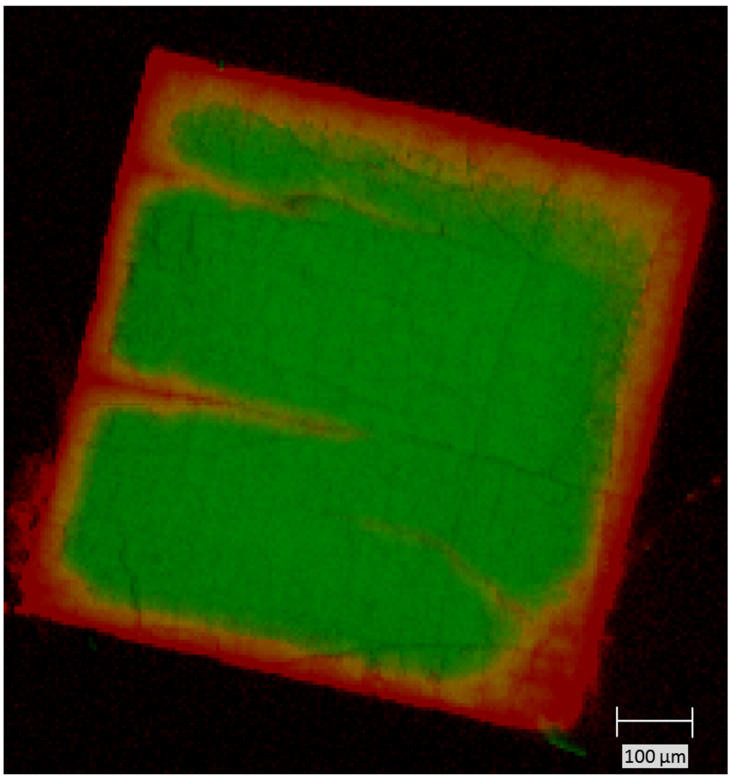

Figure 3.4. Raman map of ligand exchange in MOF-5 using 0.1 M solution of H_2BDC-d_4 in DMF after 1 day. Incorporation of the ligand (H_2BDC-d_4, red) occurs mostly along the exterior of the crystal with the rest of the crystal composed of BDC (green). Notably, incorporation of H_2BDC-d_4 also occurred along cracks in the crystal allowing for avenues of ligand incorporation in the interior of the crystal.

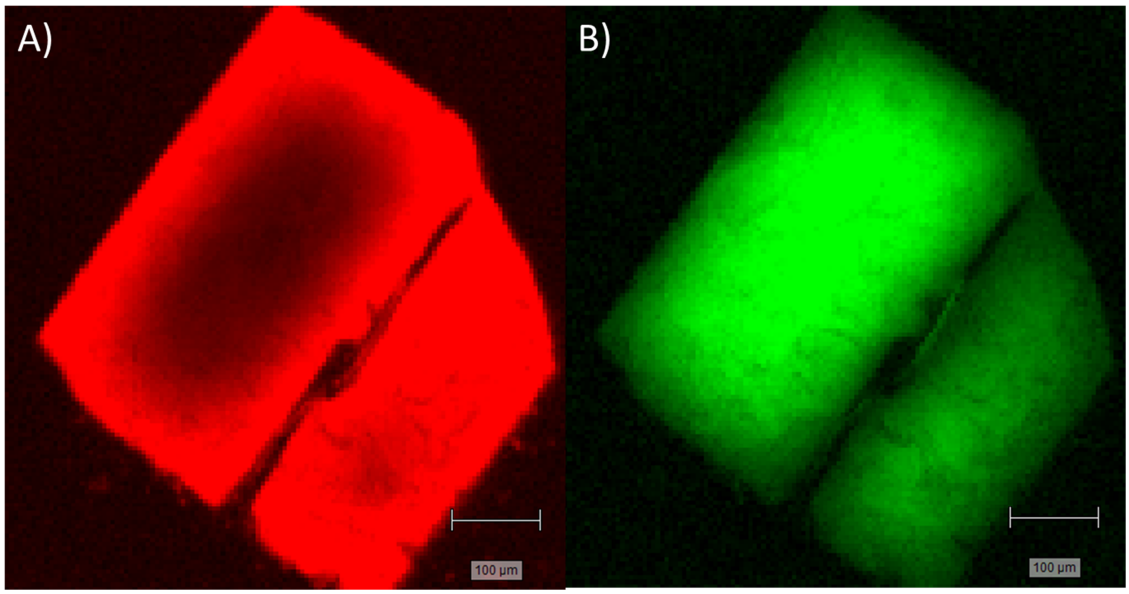

Figure 3.5. Raman maps of ligand exchange in MOF-5 using 0.1 M solution of H_2BDC-d_4 in DMF after 3 days. The incorporation of BDC-d_4 (A) is shown to occur throughout the crystal with a gradient from the outside of the crystal and along the crack towards the center with the highest concentration on the surface while (B) shows the reverse of the gradient with the highest concentration BDC at the inner areas of the crystal.

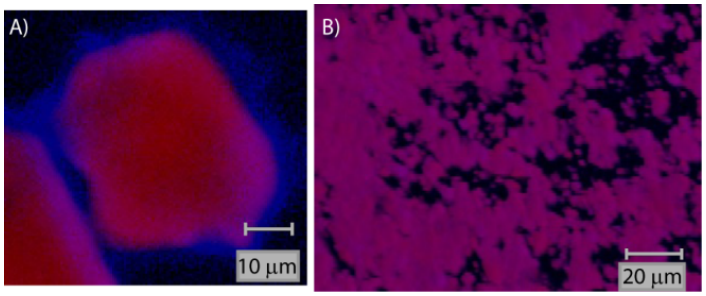

Figure 3.6. 2D Raman maps of UiO-66 showing the distribution of exchanged linkers in a sectioned single crystal of UiO-66 (blue – BDC-d_4, red – BDC, purple – mixture, A) and powder of UiO-66 (B).

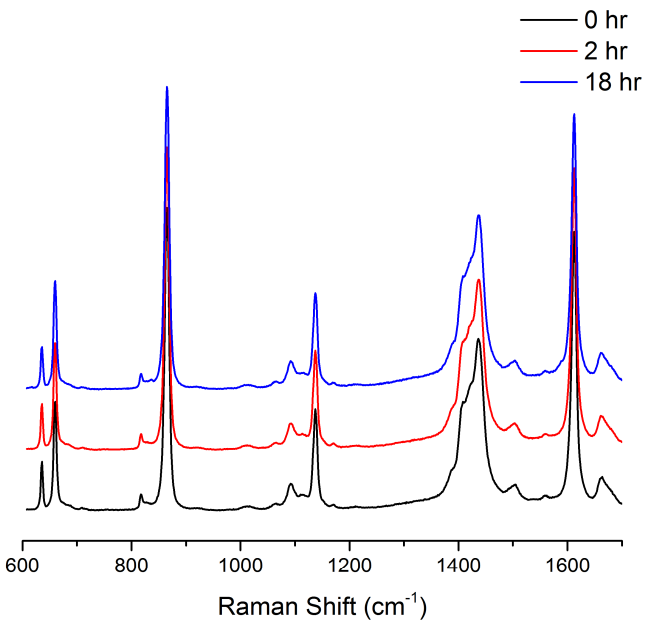

Figure 3.7. Diffusion of H_2BDC-d_4 into MOF-5. Focusing on the center of the crystal showed no H_2BDC-d_4 after 18 hours.

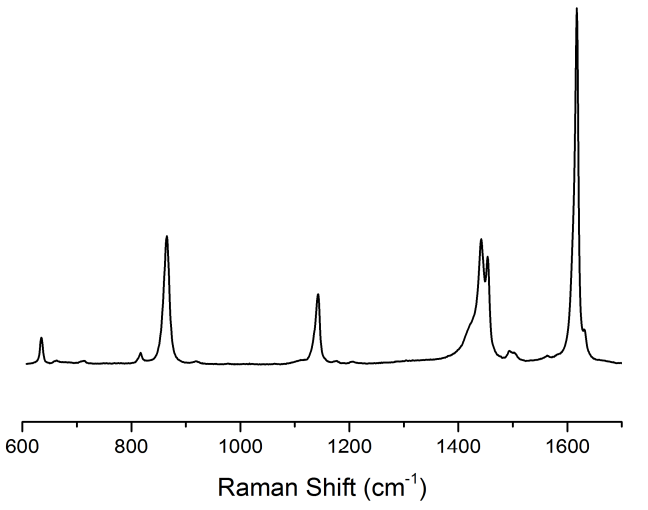

Figure 3.8. Raman spectrum of MOF-5.

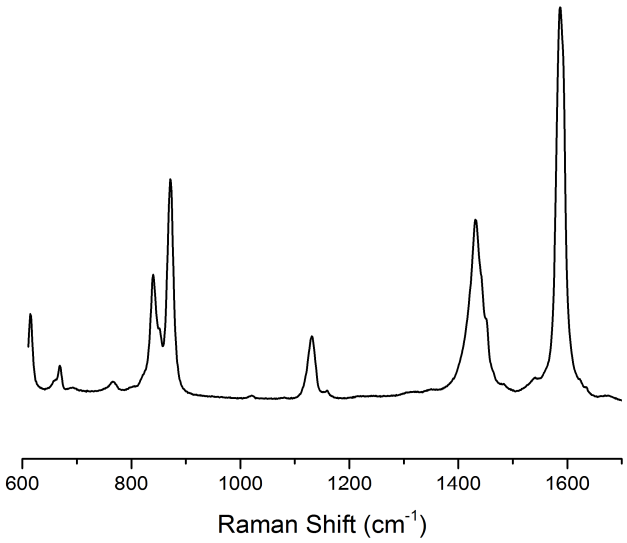

Figure 3.9. Raman spectrum of MOF-5-*d*.

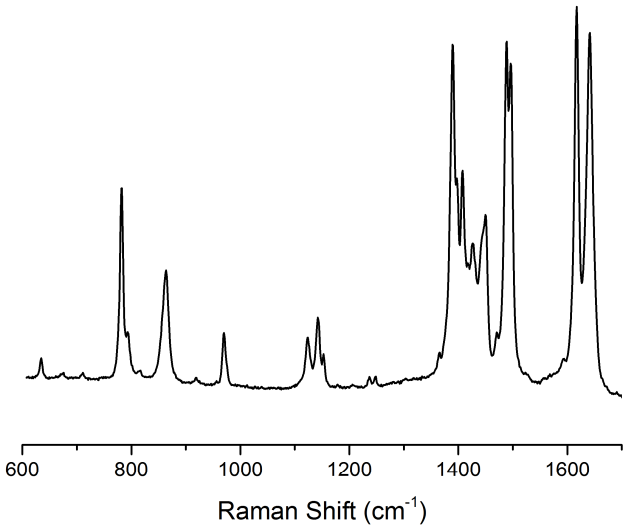

Figure 3.10. Raman spectrum of UMCM-8.

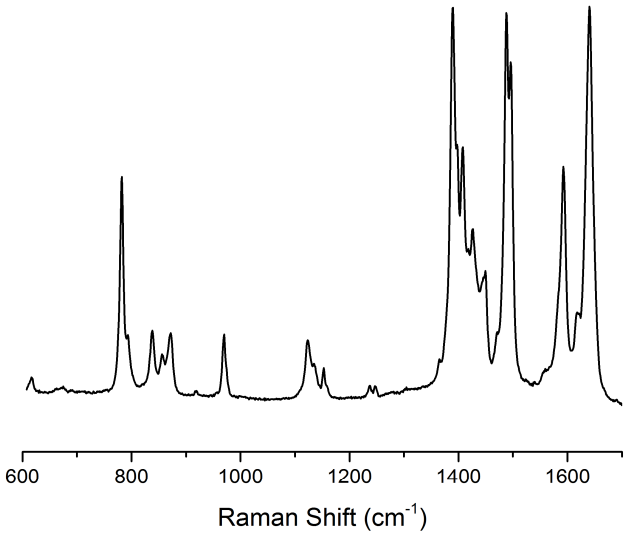

Figure 3.11. Raman spectrum of UMCM-8-*d*.

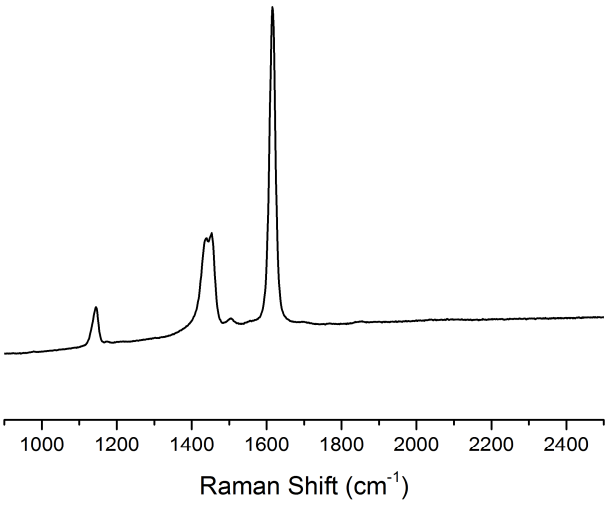

Figure 3.12. Raman spectrum of powdered UiO-66.

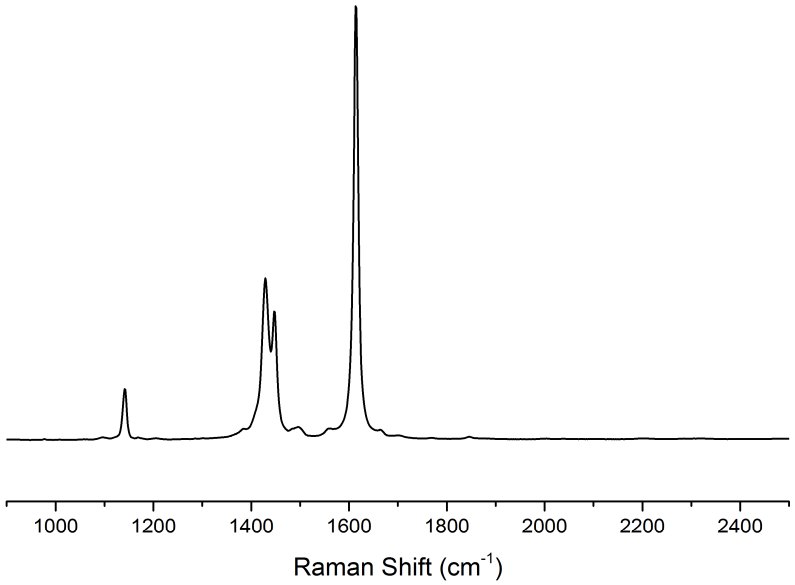

Figure 3.13. Raman spectrum of single crystals of UiO-66.

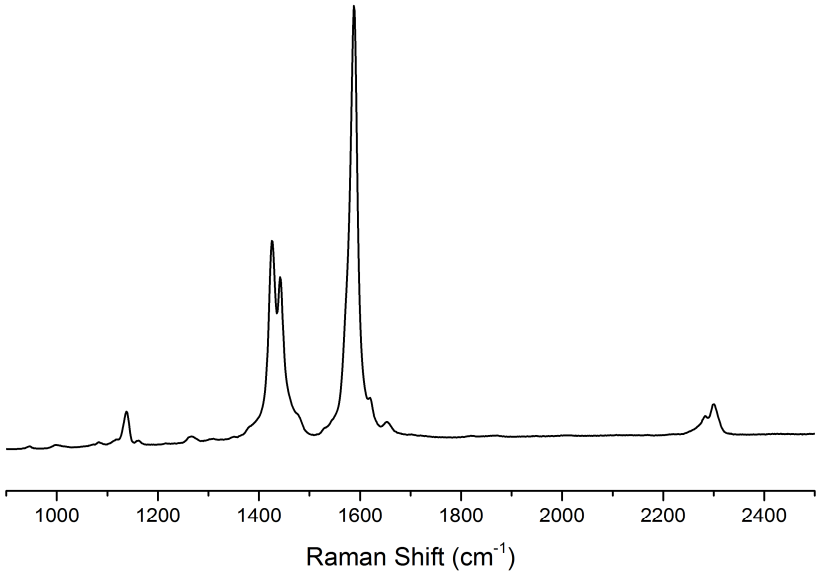

Figure 3.14. Raman spectrum of single crystals of UiO-66-*d*.

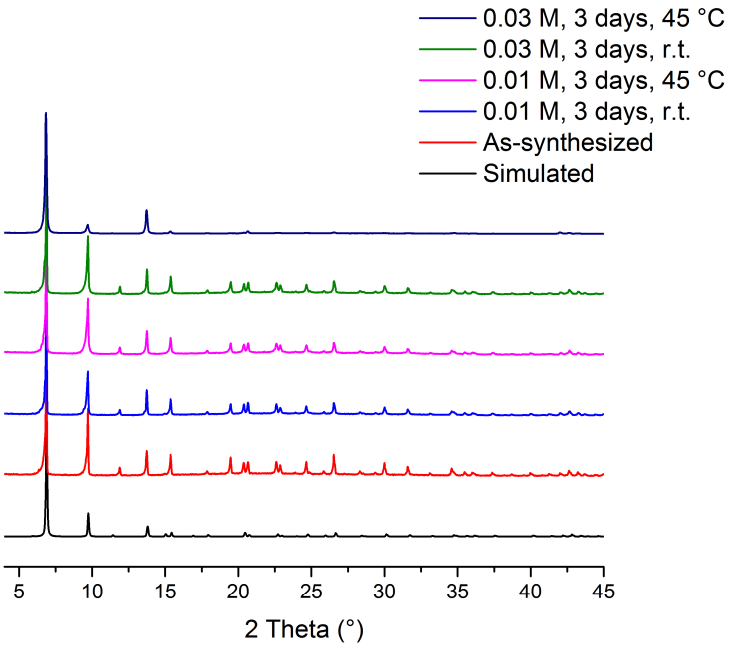

Figure 3.15. PXRD patterns of MOF-5 after exchange of 0.01 M and 0.03 M H_2BDC-d_4 in THF at room temperature and 45 °C after 3 days compared to as-synthesized and simulated MOF-5 PXRD patterns.

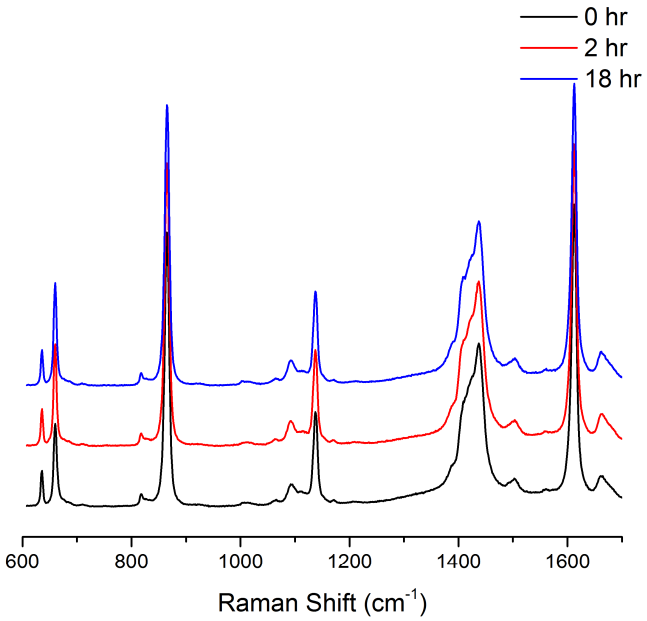

Figure 3.16. Diffusion of benzoic acid into MOF-5. Focusing on the center of the crystal showed no benzoic acid after 18 hours.

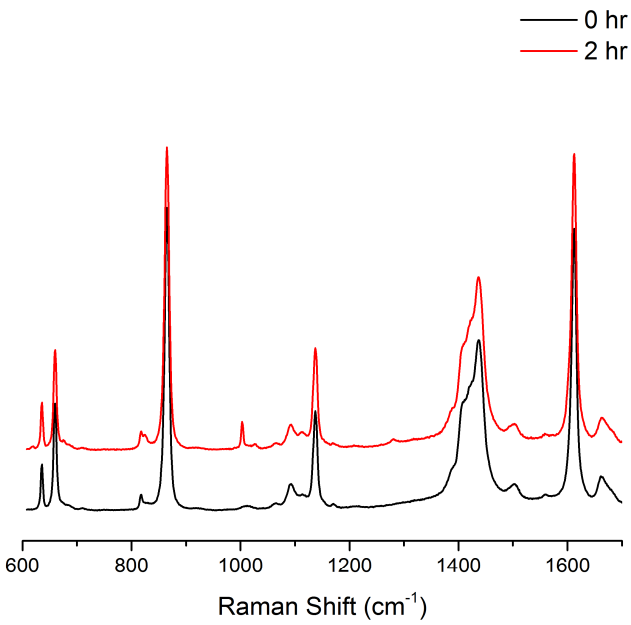

Figure 3.17. Diffusion of methyl benzoate into MOF-5. Focusing on the center of the crystal showed methyl benzoate at the center of the crystal in less than 2 hours.

3.6 Tables

Table 3.1. Average depth of exchange of BDC-d_4 into MOF-5 under various conditions in THF.

	1 equivalent (0.01 M) BDC-d_4		3 equivalents (0.03 M) BDC-d_4	
Time	Depth at 25 °C (μm)	Depth at 45 °C (μm)	Depth at 25 °C (μm)	Depth at 45 °C (μm)
18 hrs	80	150	110	185
24 hrs	120	160	145	260
72 hrs	160	205	220	280

Table 3.2. Average depth of exchange of BDC-d_4 into MOF-5 under various conditions with 0.01 M of H_2BDC-d_4 in DMF.

Time	Depth at 25 °C (μm)
18 hrs	85
24 hrs	120
48 hrs	175

Table 3.3. Average depth of exchange of BDC-d_4 into UMCM-1 under various conditions in THF.

Time	Depth with 1 equivalent (0.01 M) BDC-d_4 (μm)	Depth with 3 equivalents (0.03 M) BDC-d_4 (μm)
30	40	50
1 hr	60	80

3.7 References

(1) Burnett, B. J.; Barron, P. M.; Hu, C.; Choe, W. Stepwise Synthesis of Metal-Organic Frameworks: Replacement of Structural Organic Linkers. *J. Am. Chem. Soc.* **2011**, *133*, 9984-9987.

(2) Karagiaridi, O.; Bury, W.; Sarjeant, A. A.; Stern, C. L.; Farha, O. K.; Hupp, J. T. Synthesis and characterization of isostructural cadmium zeolitic imidazolate frameworks via solvent-assisted linker exchange. *Chem. Sci.* **2012**, *3*, 3256-3260.

(3) Kim, M.; Cahill, J. F.; Fei, H.; Prather, K. A.; Cohen, S. M. Postsynthetic Ligand and Cation Exchange in Robust Metal-Organic Frameworks. *J. Am. Chem. Soc.* **2012**, *134*, 18082-18088.

(4) Kim, M.; Cahill, J. F.; Su, Y.; Prather, K. A.; Cohen, S. M. Postsynthetic ligand exchange as a route to functionalization of 'inert' metal–organic frameworks. *Chem. Sci.* **2012**, *3*, 126-130.

(5) Li, T.; Kozlowski, M. T.; Doud, E. A.; Blakely, M. N.; Rosi, N. L. Stepwise Ligand Exchange for the Preparation of a Family of Mesoporous MOFs *J. Am. Chem. Soc.* **2013**, *135*, 11688-11691.

(6) Pereira, C. F.; Howarth, A. J.; Vermeulen, N. A.; Almeida Paz, F. A.; Tomé, J. P. C.; Hupp, J. T.; Farha, O. K. Towards hydroxamic acid linked zirconium metal-organic frameworks *Mater. Chem. Front.* **2017**, *1*, 1194-1199.

(7) Xu, Y.; Vermeulen, N. A.; Liu, Y.; Hupp, J. T.; Farha, O. K. SALE-Ing a MOF-Based "Ship of Theseus." Sequential BuildingBlock Replacement for Complete Reformulation of a Pillared-Paddlewheel Metal—Organic Framework. *Eur. J. Inorg. Chem.* **2016**, *2016*, 4345-4348.

(8) Lalonde, M. B.; Mondloch, J. E.; Deria, P.; Sarjeant, A. A.; Al-Juaid, S. S.; Osman, O. I.; Farha, O. K.; Hupp, J. T. Selective Solvent-Assisted Linker Exchange (SALE) in a Series of Zeolitic Imidazolate Frameworks. *Inorg. Chem.* **2015**, *54*, 7142.

(9) Nickerl, G.; Senkovska, I.; Kaskel, S. Tetrazine functionalized zirconium MOF as an optical sensor for oxidizing gases. *Chem. Commun.* **2015**, *51*, 2280-2282.

(10) Pullen, S.; Fei, H.; Orthaber, A.; Cohen, S. M.; Ott, S. Enhanced Photochemical Hydrogen Production by a Molecular Diiron Catalyst Incorporated into a Metal-Organic Framework. *J. Am. Chem. Soc.* **2013**, *135*, 16997-17003.

(11) Yu, X.; Cohen, S. M. Photocatalytic metal–organic frameworks for the aerobic oxidation of arylboronic acids. *Chem. Commun.* **2015**, *51*, 9880.

(12) Liu, C.; Zeng, C.; Luo, T. Y.; Merg, A. D.; Jin, R.; Rosi, N. L. Establishing Porosity Gradients within Metal-Organic Frameworks Using Partial Postsynthetic Ligand Exchange. *J. Am. Chem. Soc.* **2016**, *138*, 12045-12048.

(13) McGuire, C. V.; Forgan, R. S. The surface chemistry of metal–organic frameworks. *Chem. Commun.* **2015**, *51*, 5199-5217.

(14) Fluch, U.; Paneta, V.; Primetzhofer, D.; Ott, S. Uniform distribution of post-synthetic linker exchange in metal-organic frameworks revealed by Rutherford backscattering spectrometry. *Chem. Commun.* **2017**, *53*, 6516-6519.

(15) Li, H.; Eddaoudi, M.; O'Keeffe, M.; Yaghi, O. M. Design and synthesis of an exceptionally stable and highly porous metal-organic framework. *Nature* **1999**, *402*, 276-279.

(16) Gross, A. F.; Sherman, E.; Mahoney, S. L.; Vajo, J. J. Reversible Ligand Exchange in a Metal-Organic Framework (MOF): Toward MOF-Based Dynamic Combinatorial Chemical Systems. *J. Phys. Chem. A* **2013**, *117*, 3771-3776.

(17) Koh, K.; Van Oosterhout, J. D.; Roy, S.; Wong-Foy, A. G.; Matzger, A. Exceptional surface area from coordination copolymers derived from two linear linkers of differing lengths. *J. Chem. Sci.* **2012**, *3*, 2429-2432.

(18) Cavka, J. H.; Jakobsen, S.; Olsbye, U.; Guillou, N.; Lamberti, C.; Bordiga, S.; Lillerud, K. P. A New Zirconium Inorganic Building Brick Forming Metal Organic Frameworks with Exceptional Stability. *J. Am. Chem. Soc.* **2008**, *130*, 13850-13851.

(19) Øien, S.; Wragg, D.; Reinsch, H.; Svelle, S.; Bordiga, S.; Lamberti, C.; Lillerud, K. P. Detailed Structure Analysis of Atomic Positions and Defects in Zirconium Metal-Organic Frameworks. *Crsyt. Growth Des.* **2014**, *14*, 5370-5372.

(20) Trickett, C. A.; Gagnon, K. J.; Lee, S.; Gandara, F.; Burgi, H. B.; Yaghi, O. M. Definitive Molecular Level Characterization of Defects in UiO-66 Crystals. *Angew. Chem. Int. Ed. Engl.* **2015**, *54*, 11162-11167.

(21) Koh, K.; Wong-Foy, A. G.; Matzger, A. J. MOF@MOF: microporous core-shell architectures. *Chem. Commun.* **2009**, *0*, 6162-6164.

(22) Katz, M. J.; Brown, Z. J.; Colon, Y. J.; Siu, P. W.; Schiedt, K. A.; Snurr, R. Q.; Hupp, J. T.; Farha, O. K. A facile synthesis of UiO-66, UiO-67 and their derivatives. *Chem. Commun.* **2013**, *49*, 9449-9451.

(23) NIST Computational Chemistry Comparison and Benchmark Database NIST Standard Reference Database Number 101 Release 18, October 2016, http://cccbdb.nist.gov/ (accessed February 10, 2017)

Chapter 4

Histamine Incorporation into Zeolitic Imidazolate Frameworks for Capture of CO_2

4.1 Introduction

Global CO_2 levels continue to rise as populations and industries across the world grow using power mainly derived from fossil fuels. This will have catastrophic effects on the environment from increases in air pollution to the increase in global temperatures and the subsequent rising of sea levels.[1] To stem this issue, CO_2 capture and sequestration methods have been researched and developed over the years.[2] These methods have included, among others, the use of conventional sorbents such as alumina, silica, and activated carbons and aqueous alkanolamines. The common issue is that with existing sorbents the cost of capture is too great to be widely deployed.[3] The single greatest cost is associated with capture and regeneration of the sorbent used to selectively remove the CO_2 from the other (more abundant) components in the flue gas stream. Thus the problem of sorbent development is a central one for the success of CO_2 reduction strategies especially in the case of coal-fired power plants, the largest point source of CO_2 emission.[4] Although alkanolamines have great selectivity for CO_2 and are able to uptake large quantities even at low partial pressures of CO_2 due to reactive adsorption, these advantages are offset by the relatively low capacity for CO_2 when compared to the theoretical maximum for sorbent materials and by the difficulty in regeneration of spent alkanolamine.[5] This difficulty arises from the elevated temperatures required for regeneration that can result in decomposition of the alkanolamine solution.

MOFs are a relatively new class of porous materials that have shown promise for the storage and separation of gases such as H_2, methane, and CO_2.[6-8] This is in large part due to the high surface areas of MOFs as well as the various strategies to introduce tunability into the materials. This allows for the design of MOFs to suit specific applications by altering the chemical and physical characteristics of the MOF. Development of MOFs for CO_2 capture has focused on discovering materials that possess specific sites for selective adsorption.[5] While

MOFs that do not possess selective sites can adsorb large quantities of CO_2 (typically at very high pressures), this does little to aid efforts for CO_2 capture from point sources or from ambient air. This is due to the nature of the physisorption process that is not chemically selective and other gases, nitrogen in particular for flue gas, will compete to adsorb to the MOF. Some MOFs that possess coordinatively unsaturated metal sites will impart selectivity through coordination of CO_2 overcoming the issue of competition from N_2; however, there are some drawbacks that should be noted. The prime issue is that while CO_2 can be selectively adsorbed over N_2, other gases that may be present in the application such as water vapor can also coordinate to the coordinatively unsaturated metal center eroding capacity and sometimes contributing to sorbent degradation.[9] Other attempts to impart selectivity have focused on amine bearing linkers that would act in a manner similar to alkanolamines or ammonia in chemisorption of CO_2.

To accomplish the incorporation of amines, there are primarily three methods that have been used in the literature that have seen varying degrees of success. The first is by direct incorporation of an amine bearing linker during MOF synthesis; however this typically can only be carried out with aniline derivatives.[10] While this has succeeded in the incorporation of amines into MOFs, anilines are not as capable for the chemisorption of CO_2 as alkylamines. For instance, 2-aminoterephthalate in IRMOF-3 improves the uptake of CO_2 by only 0.1 wt% when compared to the nonfunctionalized material.[11] The second approach takes advantage of coordinatively unsaturated metal centers present in some MOFs to append ligands that possess primary or secondary amines to these centers (e.g. ethylene diamine).[12] This has proven successful for the incorporation of primary amines into MOFs and has been shown to significantly increase CO_2 uptake at nearly atmospheric partial pressures albeit with the potential for leaching the small molecule diamines from the sorbent. The third method utilizes postsynthetic modification to react a linker already in the MOF to add an alkyl amine directly tethered to the linker.[12] Alternatively, postsynthetic methods can be used to deprotect a protected amine. Specifically, it has been shown that a ligand bearing a boc-protected L-proline can be thermally deprotected to reveal the secondary amine which has been utilized in catalysis.[13, 14]

If the goal in using MOFs in CO_2 removal is for betterment of the environment, it is important to consider the environmental footprint of MOF synthesis. To this end, the most commonly employed ligands present a challenge as they are typically derived from petroleum

based sources and will have issues with renewability and carbon footprint. There are currently only a few examples of MOFs synthesized from small molecules obtained from more sustainable methods such as through direct production by biological systems or fermentation of biological products.[15] In an effort to both capture CO_2 effectively and use molecules derived from more environmentally sustainable sources, we came upon a different method for functionalizing MOFs with primary amines for CO_2 capture: postsynthetic exchange (PSE).

PSE is a recently developed method of MOF functionalization frequently utilized in the incorporation of ligands into MOFs that would otherwise be impossible to incorporate through standard solvothermal synthesis methods.[16] Typically, PSE is conducted by immersing the parent MOF in a solution containing the functionalized ligand combined with agitation and/or gentle heating. The ligands exchanged into the MOF tend to have the same linker geometry as is present in the parent MOF allowing for direct replacement of framework linkers with ligands in solution. Zeolitic imidazolate frameworks (ZIFs) are among the first materials PSE was studied on showing that imidazolates in the framework were easily replaceable for functionalized imidazole in solution.[17] ZIFs are a subset of MOFs that are comprised of single metal ions (typically zinc or cobalt) that are bridged tetrahedrally to 4 imidazole based linkers to form an overall zeolitic structure.[18] ZIF-8 is the prototypical ZIF system, composed of zinc ions bridged by 2-methylimidazole, due to its relative ease of synthesis and its purported hydrolytic stability. In looking at the types of functionalized imidazoles, histamine stands out as a promising linker as not only does it possess a primary amine that should be amenable to CO_2 adsorption but it also is a readily available biomolecule. PSE in ZIF-8 has already been extensively studied with non-amine bearing linkers and has been shown to proceed under mild conditions.[19] Incorporation of histamine into ZIF-8 is expected to have a profound effect on CO_2 adsorption and due to its mild conditions, PSE will be utilized. In addition to ZIF-8 another ZIF was selected for incorporation of histamine: ZIF-70. ZIF-70 is a mixed linker systems based on imidazole and nitroimidazole possessing extremely large pores among ZIFs and a high surface area relative to ZIF-8 which may allow for better adsorption kinetics.[20]

4.2 Results and Discussion

ZIF-8 was the first material extensively studied for the incorporation of histamine for a number of reasons. Chiefly, it is the most well studied of the ZIFs with both simple and scalable synthesis procedures that are amenable to large scale deployment. Additionally, its high thermal and chemical stability relative to the other ZIFs studied herein was ideal for testing the systems for PSE of histamine. Based upon procedures for incorporation of non-amine bearing imidazoles into ZIF-8 developed by Cohen and coworkers, attempts at incorporation through PSE was conducted with histamine in methanol at 65 °C.[19] Incorporation of histamine occurred and the material maintained its crystallinity. However, results were inconsistent and it was observed that a significant portion of the ZIF-8 had decomposed over the course of the reaction due to significant losses in mass of the material. A different procedure utilizing N,N-dimethylformamide (DMF) was developed which resulted in a ZIF-8 derivative with 50 mol% incorporation of histamine referred to as Hist@ZIF-8. Hist@ZIF-8 was observed to maintain the crystallinity of its parent ZIF-8 by powder X-ray diffraction (PXRD). Isothermal N_2 adsorption experiments revealed that the Braunnaur-Emmett-Teller (BET) surface area had decreased from 1388 m^2/g to 1174 m^2/g which is expected as the incorporation of more bulky linkers into MOFs typically results in a decrease in surface area. Isothermal CO_2 adsorption experiments were conducted on Hist@ZIF-8 at 25 °C and showed an increase in total uptake with a maximum of 5.6 wt% at 1 bar compared to 3.5 wt% for ZIF-8 under the same conditions. It is important to note for this material, that half of the total uptake occurs before 0.01 bar CO_2 and under this regime (0.001-0.01 bar) that the uptake of CO_2 is slow with equilibrium being achieved over multiple hours. Hist@ZIF-8 also did not completely release all adsorbed CO_2 upon evacuation after completion of the CO_2 adsorption experiment. Thermogravimetric analysis (TGA) of the material after evacuating Hist@ZIF-8 after CO_2 adsorption experiments showed a mass loss of 7.9 wt% before 280 °C which is consistent with a ratio of 0.5 mol CO_2:1 mol histamine in the MOF. Adsorption of CO_2 by ethanolamine follows a mechanism whereby 2 molecules of ethanolamine react with 1 molecule of CO_2 to generate the carbamate ammonium salt which can be removed by heating to 100-120 °C. This is in agreement with what is observed upon CO_2 adsorption in Hist@ZIF-8. Conducting the isothermal CO_2 adsorption experiments at elevated temperatures showed minimal loss of capacity, decreasing to 4.5 wt% at 70 °C, and maintaining similar low pressure adsorption behavior. Regeneration of the material was also accomplished by

heating Hist@ZIF-8 under dynamic vacuum for 18 hours at 140 °C. Subsequent isothermal CO_2 adsorption experiments showed no loss in CO_2 capacity after activation.

Following the successful incorporation of histamine into ZIF-8, attempts were made at incorporating histamine into ZIF-70. ZIF-70 showed complete degradation upon prolonged exposure to ligand exchange conditions used above. Further dilution of histamine in the exchange solution resulted in no appreciable incorporation. Through the course of the ligand exchange studies with ZIF-8 above, concern was raised over the possible effect the primary amine might have on the integrity of the MOF and if it were possible that chelation of the metal with histamine would result in degradation of the MOF. While this was not observed with ZIF-8, it does not mean that the primary amine would always be innocent in the PSE experiments and indeed it appears that this is a primary factor for the degradation of ZIF-70. Acetyl protection of the primary amine histamine provided a simple experiment to test the influence of the primary amine on the degradation and it was found that incorporation of Nω-acetylhistamine was possible using PSE yielding a material with ~36 mol% incorporation known as AcetylHist@ZIF-70. While thermal deprotection of acetamides is possible, TGA showed that a mass loss is observable at 300 °C in pure ZIF-70 and indeed, no other mass loss attributable to loss of acetyl was observed in AcetylHist@ZIF-70.

Other protecting groups for amines are readily available and in particular tertbutoxycarbamide is desirable as it is readily thermally deprotected and has already been used in other MOFs to conceal amines until after incorporation.[13,14] Attempts at incorporating tert-butyl (2-(1H-imidazol-4-yl)ethyl)carbamate into ZIF-70 were mildly successful following conditions above resulting in 10 mol% incorporation into the ZIF based on imidazole (BocHist@ZIF-70). With no loss in crystallinity observed after incorporation, TGA showed a mass loss of 4.7% with onset at 175 °C commensurate with thermal deprotection of histamine. Attempts at thermal deprotection under dynamic vacuum have so far proven unsuccessful with heating at 200 °C resulting in decomposition of the material in addition to removal of the t-butoxycarbonyl and heating at 175 °C resulting in no loss of crystallinity but no noticeable deprotection.

4.3 Conclusion and Future Directions

Postsynthetic exchange was used to incorporate a primary amine bearing imidazole, histamine, into ZIF-8. The modified material Hist@ZIF-8 was shown to have improved CO_2 capacity compared to the parent ZIF-8 and in particular showed higher low pressure uptake. This has shown the potential for histamine to be utilized in the synthesis and design of ZIFs allowing for tailoring towards CO_2 capture or potentially other small molecules. Attempts at modifying other ZIFs with histamine were met with failure due to the presumed reactivity of the primary amine on the linker. Protecting the primary amine with acetyl and t-butoxycarbonyl moieties to stymie reactivity allowed for successful incorporation of these modified histamines into ZIF-70. Attempts at removing the protecting groups after incorporation into ZIF-70 have to date been unsuccessful.

Further advancement towards incorporation of histamine into ZIFs diverge into a number of paths. While PSE was explored here exclusively for the incorporation of histamine or its protected forms, it is possible to conceive of a pathway for inclusion that uses these ligands in direct synthesis of the ZIFs in question. While histamine on its own is expected to be problematic for solvothermal ZIF synthesis, its derivatives are promising in this regard. The groups of Telfer and Kaskel have both shown that despite the thermal sensitivity of t-butoxycarbonyl protected amines, this protecting group is stable to a number of solvothermal conditions used in MOF synthesis.[13, 14] It is thus likely that conditions for direct incorporation of boc-protected histamine through solvothermal methods exist and this would provide for a straightforward method towards integration of histamine into other ZIFs.

4.4 Experimental Methods

Materials: All reagents were purchased from commercial vendors and used without further purification unless otherwise noted. ZIF-8 was purchased from Sigma Aldrich as Basolite® Z1200.

Thermogravimetric Analysis: A Q50 TGA (TA instruments) was used for thermogravimetric data. Samples were heated in a platinum pan under flowing, dry N_2.

Gas sorption measurements: N_2 sorption isotherms were carried out using a NOVA 4200e (Quantachrome Instruments) and CO_2 sorption isotherms were carried out using an

Autosorb iq2 (Quantachrome Instruments). N_2 (99.999%) and bone-dry CO_2 (99.9%) were purchased from Cryogenic Gases. Activated samples were placed into sample cells under N_2 atmosphere and transferred to the instruments for measurements at 77K (N_2) and 298K or 343K (CO_2).

Powder X-ray diffraction: Powder X-ray diffraction (PXRD) data were collected at ambient temperature on a PANalytical Empyrean diffractometer in Bragg–Brentano geometry using Cu-Kα radiation (1.54187 Å) operating at 45 kV, 40 mA. The incident beam was equipped with a Bragg-BrentanoHD X-ray optic using fixed slits/soller slits. The detector was a silicon-based linear position sensitive X'Celerator Scientific operating in 1-D scanning mode. Data were collected from 3° to 45° 2θ using a step size of 0.0167° 2θ and a count time of at last 10 s per step.

Nω-(tertbutoxycarbonyl)-histamine synthesis:

tert-Butyl 4-(2-((tert-butoxycarbonyl)amino)ethyl)-1H-imidazole-1-carboxylate: Histamine (2.22 g, 20 mmol) was added to a 500 mL round-bottom flask with 200 mL of THF and 50 mL of MeOH. Then, di-tert-butyl dicarbonate (10.4 g, 48 mmol) was added and the solution was stirred at room temperature overnight. The reaction mixture was evaporated to dryness and purified via silica gel column chromatography with 1:1 EtOAc:Hexanes. The product was isolated as a white powder. Yield: 3.86 g, 62 %. ^{1}H NMR (400 MHz, $CDCl_3$, ppm) δ 7.97 (*s*, 1H) 7.11 (*s*, 1H) 3.39 (*m*, 2H) 2.70 (*m*, 2H) 1.59 (*s*, 9H) 1.41 (*s*, 9H).

tert-butyl (2-(1H-imidazol-4-yl)ethyl)carbamate: 4-(2-((tert-butoxycarbonyl)amino)ethyl)-1H-imidazole-1-carboxylate (1.80 g, 5.7 mmol) was added to a 250 mL round-bottom flask with 100 mL of water and 4 mL of 1,4-dioxane. The suspension was heated at 95 °C with stirring until the solution became clear and no starting material was detected by TLC (~2 hours). The product was extracted from the aqueous mixture with DCM. The organic layer was dried with $MgSO_4$, filtered, and evaporated. The resulting oil was dissolved in 20 mL of DCM and the product crystalized by layering with hexanes. The product was isolated as white needle crystals. Yield: 0.958 g, 80 %. ^{1}H NMR (400 MHz, $CDCl_3$, ppm) δ 7.54 (*s*, 1H) 6.79 (*s*, 1H) 3.38 (*m*, 2H) 2.77 (*m*, 2H) 1.40 (*s*, 9H).

ZIF-70 synthesis: ZIF-70 was synthesized by modification of procedures by Yaghi and coworkers.[20] In a 20 mL scintillation vial, $Zn(NO_3)_2 \cdot 6H_2O$ (238 mg, 0.80 mmol), imidazole (68 mg, 1.0 mmol), and 2-nitroimidazole (113 mg, 1 mmol) were dissolved in 14 mL of anhydrous DMF with sonication. The vial was capped with a Teflon lined cap and heated in a heating block at 110 °C for 4 days. After, the vial was removed from the heat block and the colorless crystals were washed with 3 × 15 mL of DMF and 3 × 15 mL of MeOH. The ZIF-70 crystals were then activated by heating at 85 °C under dynamic vacuum for 48 hours. Crystals were stored under N_2 atmosphere in a glove box until further experiments.

Ligand Exchange Reactions:

Hist@ZIF-8: Zn1200 (20.6 mg, 0.090 mmol) was added to a 1 dram vial. Histamine (111.2 mg, 1.0 mmol) was dissolved in 2 mL of DMF and added to Zn1200. The vial was capped with a Teflon lined cap and heated at 55 °C on a heating shaker for 8 hours. After, the powder was washed with 6 × 2 mL of DMF and then the solvent was exchanged to DCM by washing with 3 × 2 mL of DCM. The resulting powder was activated by heating at 140 °C for 18 hours under dynamic vacuum and stored under N_2 atmosphere in a glove box until further experiments.

AcetylHist@ZIF-70: ZIF-70 (24.3 mg, 0.10 mmol) was placed in a 1 dram vial with 2 mL of 0.01 M Nω-Acetylhistamine in DMF. The vial was capped and placed on a shaker overnight. The powder was then washed 6 × 2 mL of DMF and then the solvent was exchanged to MeOH by washing 3 × 2 mL of MeOH. The resulting powder was activated by heating at 85 °C for 48 hours under dynamic vacuum and stored under N_2 atmosphere in a glove box until further experiments.

BocHist@ZIF-70: ZIF-70 (23.8 mg, 0.098 mmol) was placed in a 1 dram vial with 2 mL of 0.01 M tert-butyl (2-(1H-imidazol-4-yl)ethyl)carbamate. The vial was capped and placed on a shaker overnight. The powder was then washed 6 × 2 mL of DMF and then the solvent was exchanged to MeOH by washing 3 × 2 mL of MeOH. The material was stored in MeOH until further experiments.

4.5 Figures

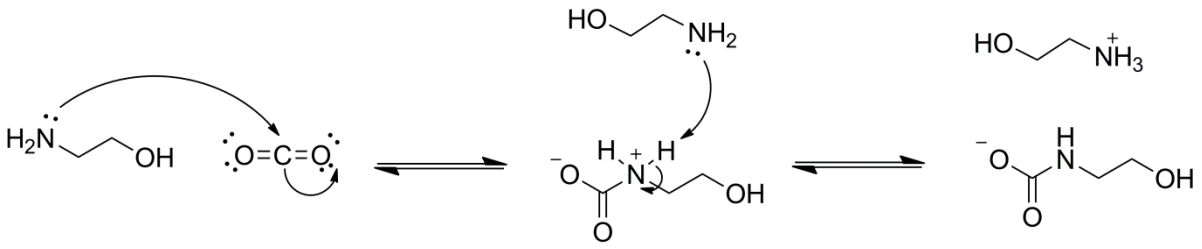

Figure 4.1. Scheme for reaction of monoethanolamine with carbon dioxide to form the carbamate salt. Two molecules of monoethanolamine are consumed per molecule of carbon dioxide.

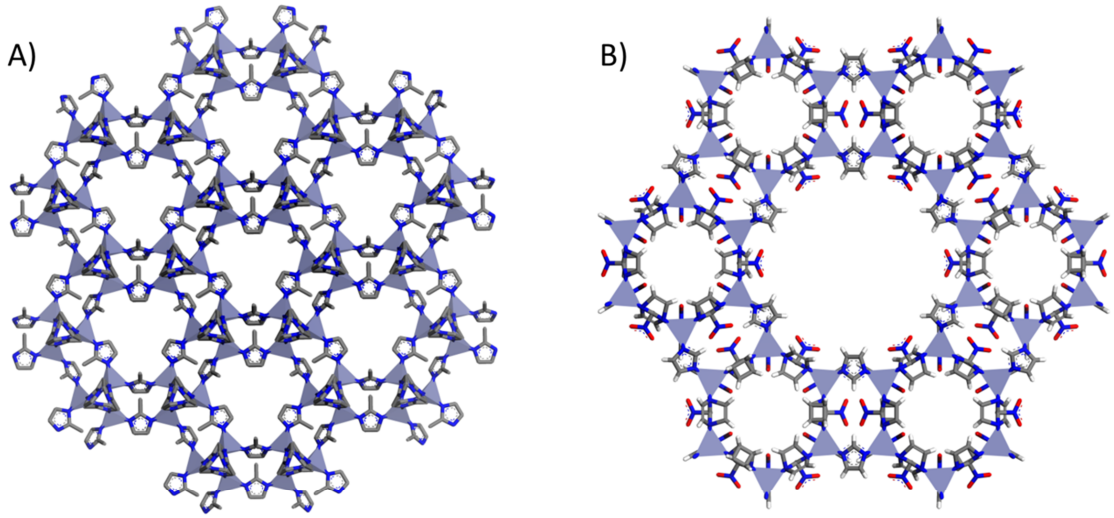

Figure 4.2. Structures of ZIF-8 (Zn(2-methylimidazole)$_2$) and ZIF-70 (Zn(imidazole)(2-nitroimidazole).

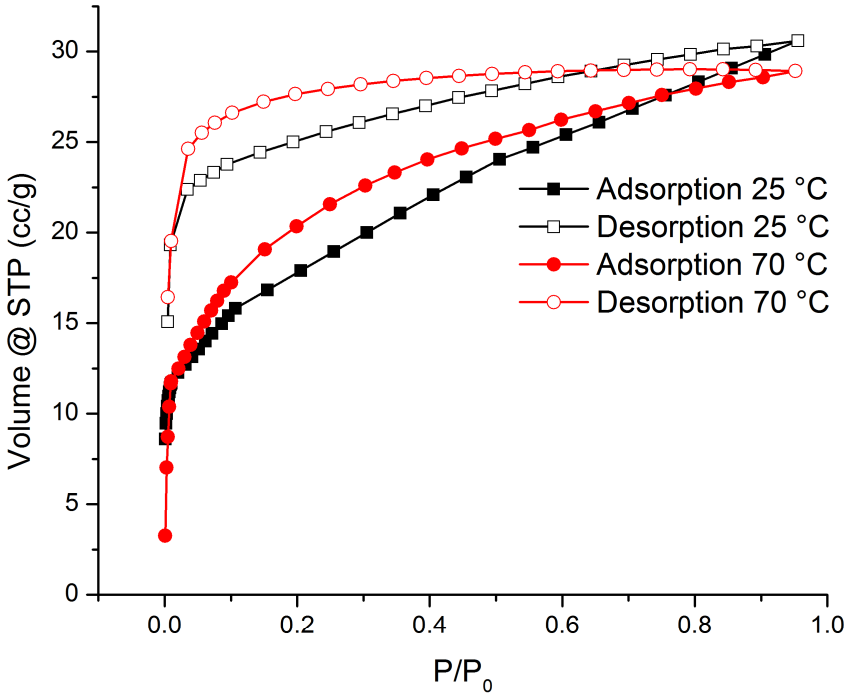

Figure 4.3. CO_2 adsorption isotherms for Hist@ZIF-8 at 25 °C (black curve) and 70 °C (red curve).

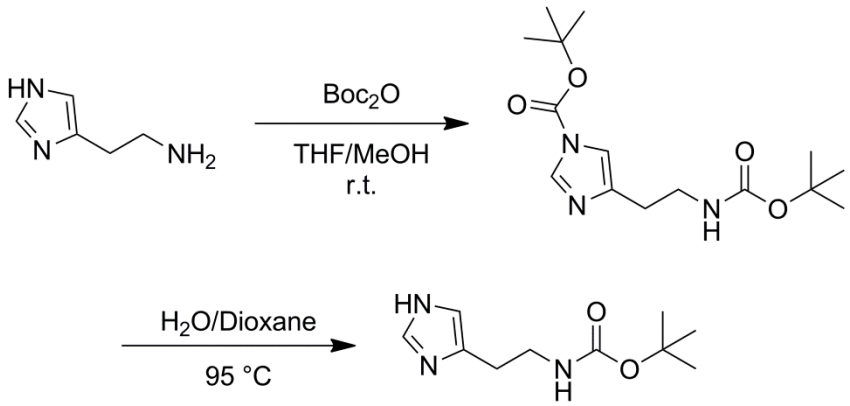

Figure 4.4. Synthetic route for synthesis of tert-butyl (2-(1H-imidazol-4-yl)ethyl)carbamate.

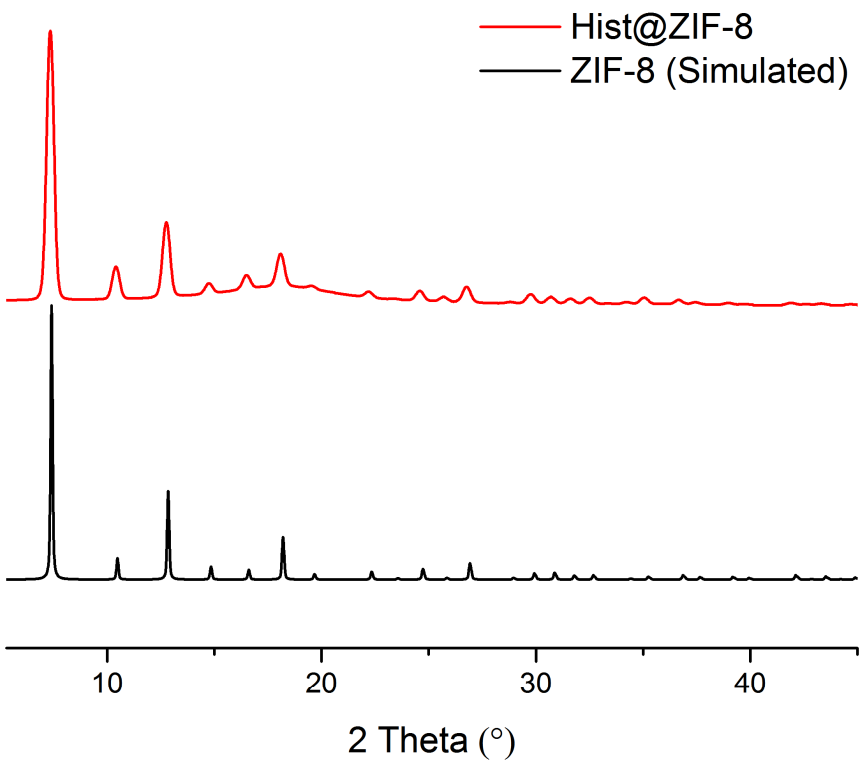

Figure 4.5. PXRD pattern of Hist@ZIF-8 compared to PXRD pattern of ZIF-8 simulated from the crystal structure.

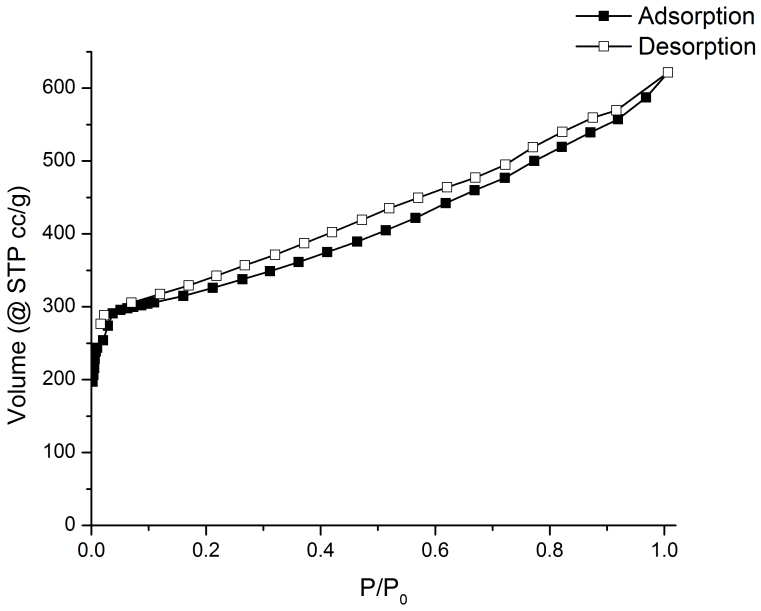

Figure 4.6. N_2 adsorption isotherm for Hist@ZIF-8 at 77K.

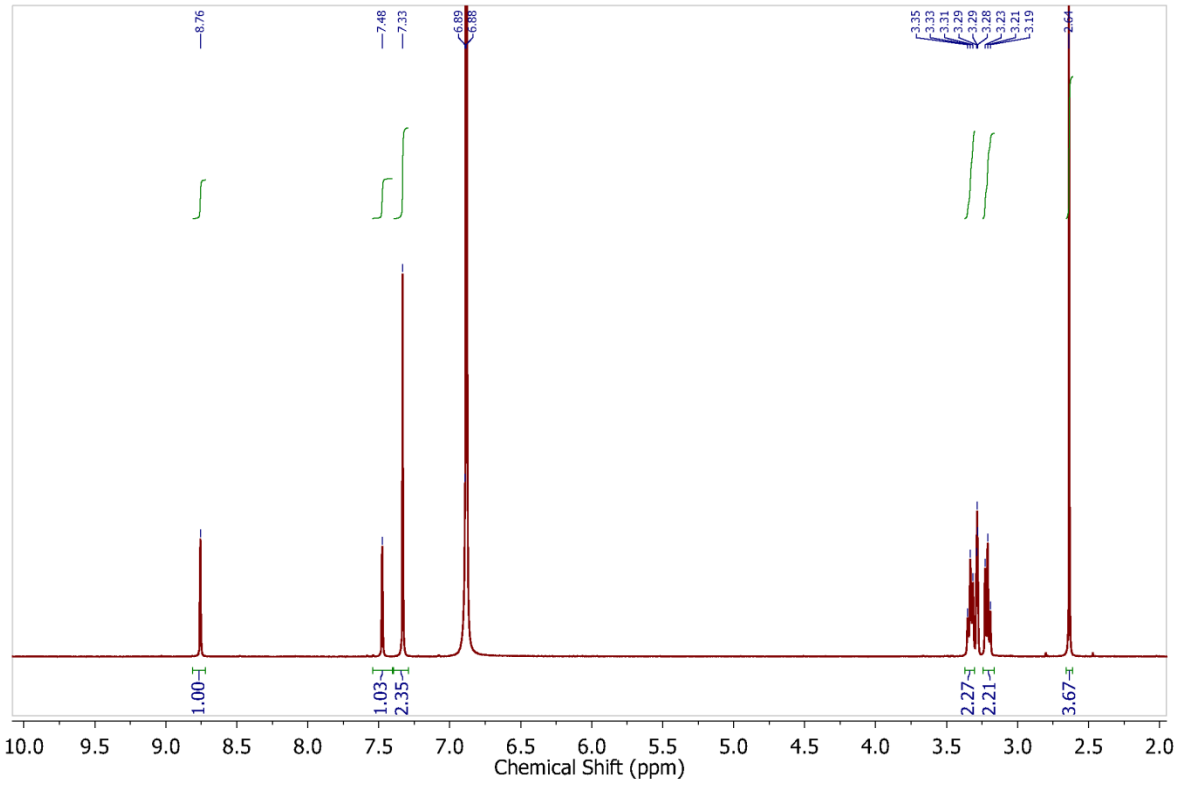

Figure 4.7. NMR spectrum of digested Hist@ZIF-8.

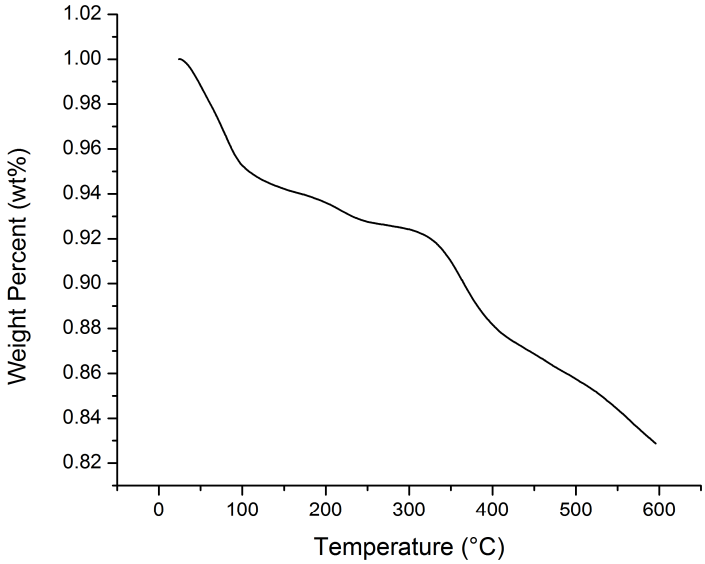

Figure 4.8. TGA trace of Hist@ZIF-8 post CO_2 adsorption isotherm.

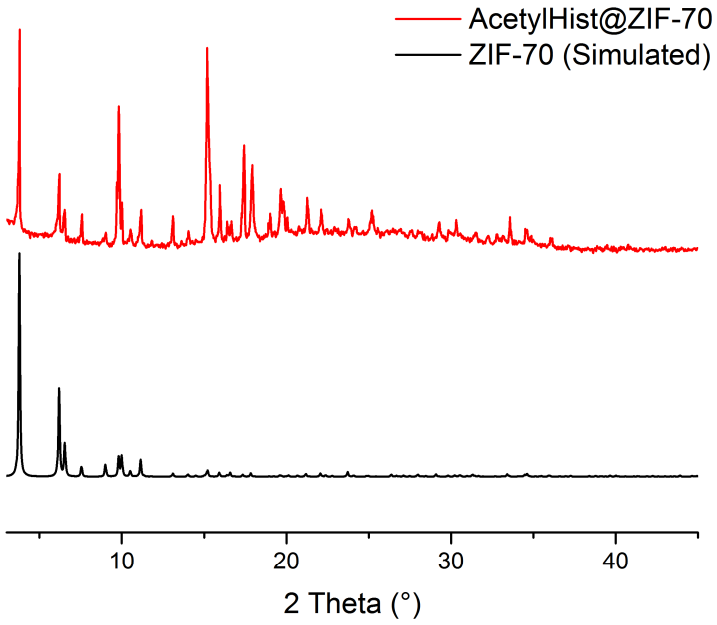

Figure 4.9. PXRD pattern of AcetylHist@ZIF-70 compared to PXRD pattern simulated from the crystal structure of ZIF-70.

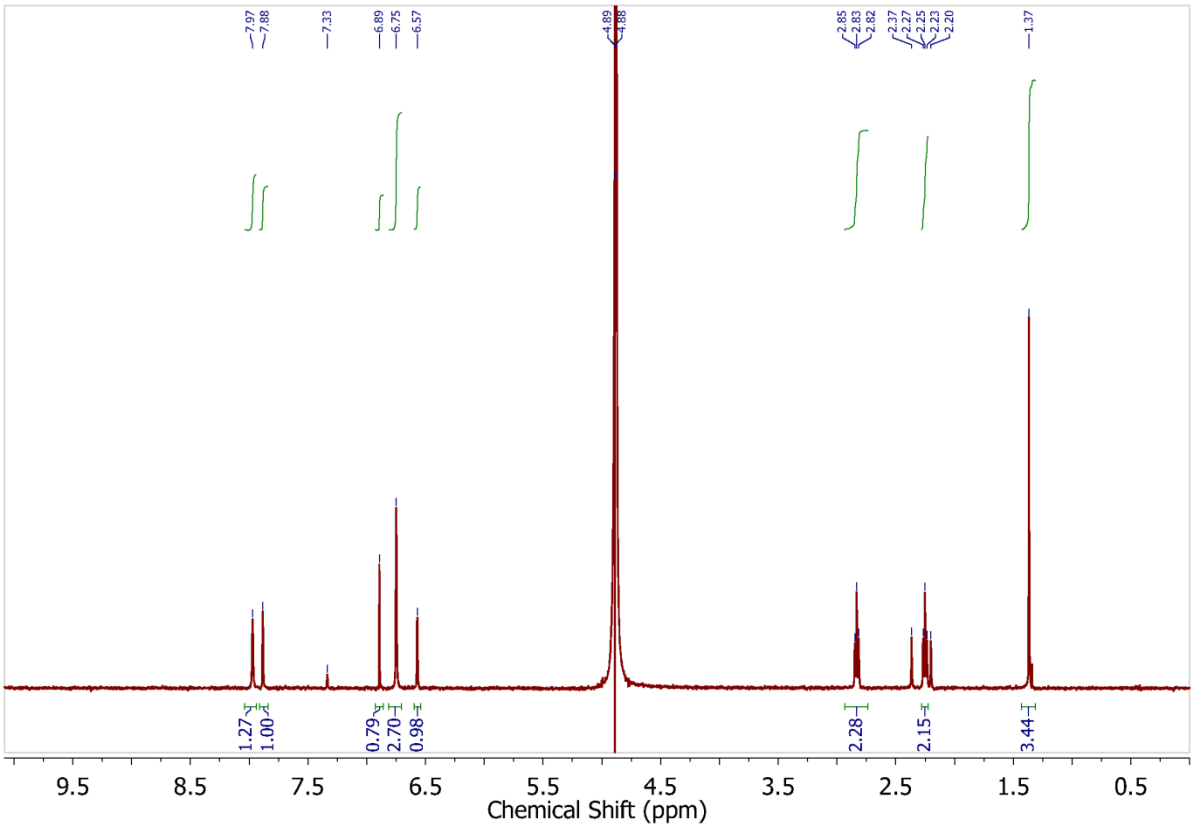

Figure 4.10. NMR spectrum of digested AcetylHist@ZIF-70.

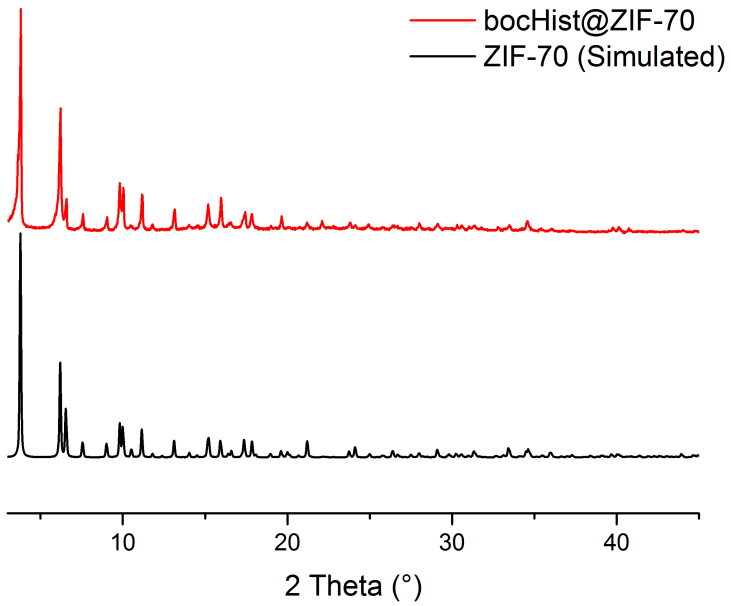

Figure 4.11. PXRD patterns of bocHist@ZIF-70 compared to PXRD pattern simulated from the crystal structure of ZIF-70.

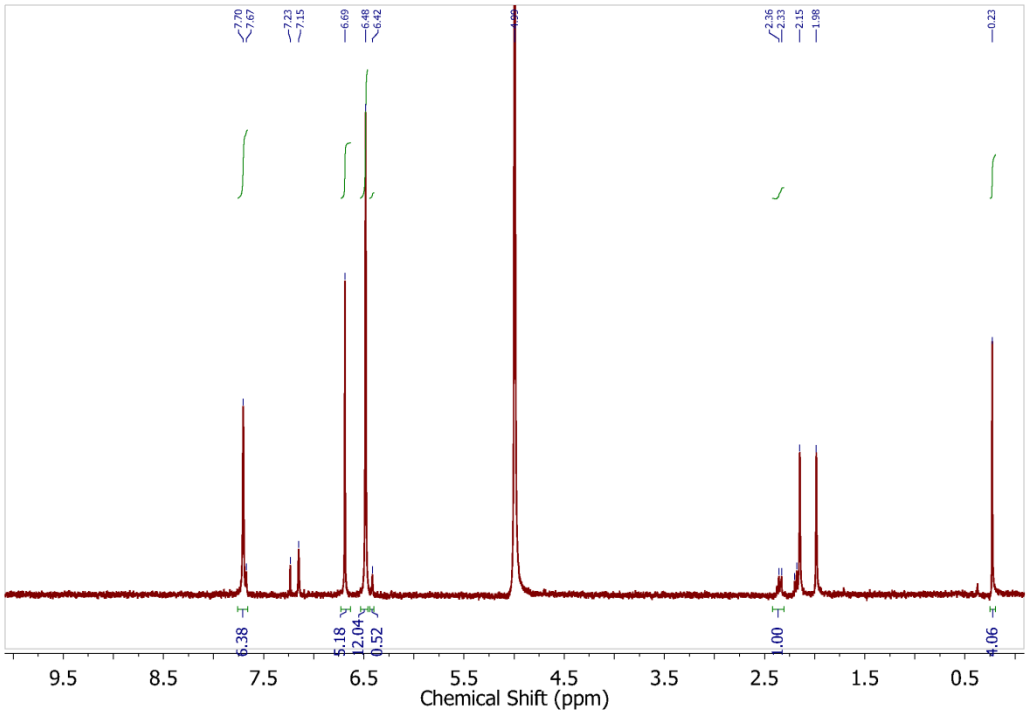

Figure 4.12. NMR spectrum of digested bocHist@ZIF-70.

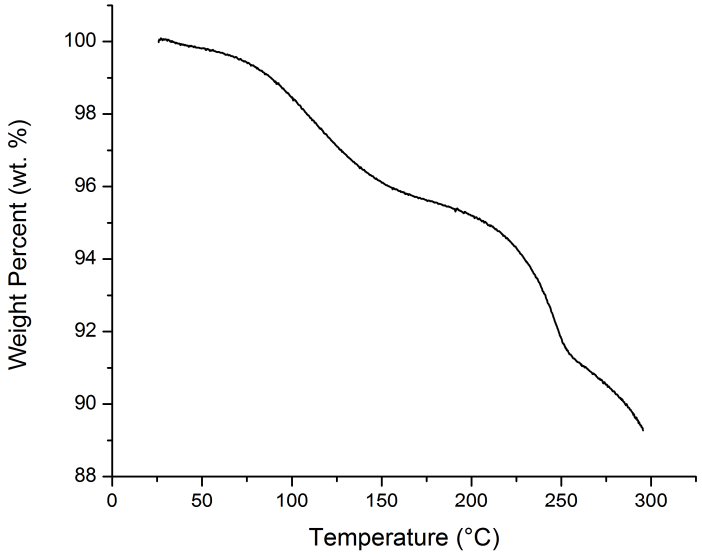

Figure 4.13. TGA trace of bocHist@ZIF-70.

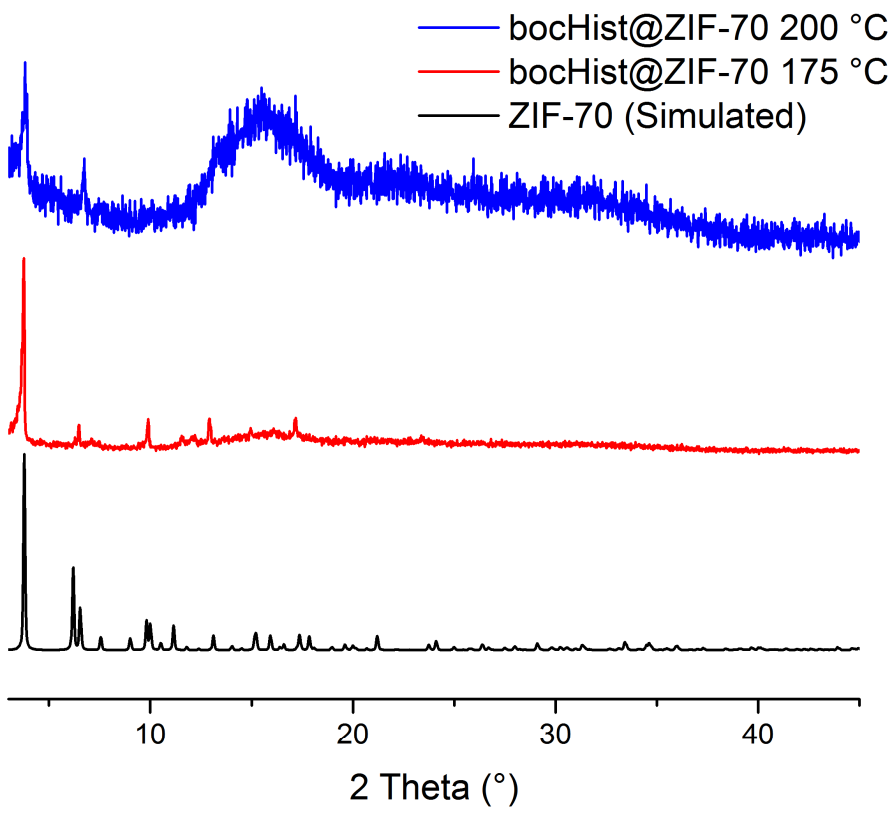

Figure 4.14. PXRD patterns of bocHist@ZIF-70 after attempted thermal deprotection at 175 °C (red curve) and 200 °C (blue curve) compared to PXRD pattern simulated from the crystal structure of ZIF-70.

4.6 References

1) Ritter, S. K. Global Warming and Climate Change. In *Chemical and Engineering News*; American Chemical Society: 2009; Vol. 87, p 11-21.

2) Lee, S.-Y.; Park, S.-J. A review on solid adsorbents for carbon dioxide capture. *J. Ind. Eng. Chem.* **2015**, *23*, 1-11.

3) Rochelle, G. T. Amine Scrubbing for CO_2 Capture. *Science*, **2009**, *325*, 1652-1654.

4)Yang, H.; Xu, Z.; Fan, M.; Gupta, R.; Slimane, R. B.; Bland, A. E.; Wright, I. Progress in carbon dioxide separation and capture: A review. *J. Environ. Sci.* **2008**, *86*, 1523-1531.

5) Sumida, K.; Rogow, D. L.; Mason, J. A.; McDonald, T. M.; Bloch, E. D.; Herm, Z. R.; Bae, T.-H.; Long, J. R. Carbon Dioxide Capture in Metal—Organic Frameworks. *Chem. Rev.* **2012**, *112*, 724-781.

6) Kayne, S. S.; Dailly, A.; Yaghi, O. M.; Long, J. R. Impact of Preparation and Handling on the Hydrogen Storage Properties of Zn4O(1,4-benzenedicarboxylate)3 (MOF-5). *J. Am. Chem. Soc.* **2007**, *129*, 14176-14177.

7) Peng, Y.; Krungleviciute, V.; Eryazici, I.; Hupp, J. T.; Farha, O. K.; Yildirim, T. Methane Storage in Metal—Organic Frameworks: Current Records, Surprise Findings, and Challenges. *J. Am. Chem. Soc.* **2013**, *135*, 11887-11894.

8) Trickett, C. A.; Helal, A.; Al-Maythalony, B. A.; Yamani, Z. H.; Cordova, K. E.; Yaghi, O. M. The chemistry of metal—organic frameworks for CO2 capture, regeneration and conversion. *Nature Reviews Materials* **2017**, *2*, 17045.

9) Kizzie, A. C.; Wong-Foy, A. G.; Matzger, A. J. Effect of Humidity on the Performance of Microporous Coordination Polymers as Adsorbents for CO2 Capture. *Langmuir* **2011**, *27*, 6368-6373.

10) Eddaoudi, M.; Kim, J.; Rosi, N.; Vodak, D.; Wachter, J.; O'Keeffe, M.; Yaghi, O. M. Systematic Design of Pore Size and Functionality in Isoreticular MOFs and Their Application in Methane Storage. *Science* **2002**, *295*, 469-472.

11) Sumida, K.; Rogow, D. L.; Mason, J. A.; McDonald, T. M.; Bloch, E. D.; Herm, Z. R.; Bae, T.-H.; Long, J. R. Carbon Dioxide Capture in Metal—Organic Frameworks. *Chem. Rev.* **2012**, *112*, 724-781.

12) McDonald, T. M.; Mason, J. A.; Kong, X.; Bloch, E. D.; Gygi, D.; Dani, A.; Crocella, V.; Giordanino, F.; Odoh, S. O.; Drisdell, W. S.; Vlaisavljevich, B.; Dzubak, A. L.; Poloni, R.; Schnell, S. K.; Planas, N.; Lee, K.; Pascal, T.; Wan, L. F.; Prendergast, D.; Neaton, J. B.; Smit, D.; Kortright, J. B.; Gagliardi, L.; Bordiga, S.; Reimer, J. A.; Long, J. R. Cooperative insertion of CO2 in diamine-appended metal—organic frameworks. *Nature* **2015**, *519*, 303-308.

13) Lun, D. J. Waterhouse, G. I. N.; Telfer, S. G. A General Thermolabile Protecting Group Strategy for Organocatalytic Metal—Organic Frameworks. *J. Am. Chem. Soc.* **2011**, *133*, 5806-5809.

14) Padmanaban, M.; Muller, P.; Lieder, C.; Gedrich, K.; Grunker, R.; Bon, V.; Senkovska, I.; Baumgartner, S.; Opelt, S.; Paasch, S.; Brunner, E.; Glorius, F.; Klemm, E.; Kaskel, S. Application of a chiral metal—organic framework in enantioselective separation. *Chem. Commun.* **2011**, *47*, 12089-12091.

15) McKinlay, A. C.; Morris, R. E.; Horcajada, P.; Ferey, G.; Gref, R.; Courvreur, P.; Serre, C. BioMOFs: Metal—Organic Frameworks for Biological and Medical Applications. *Angew. Chem. Int. Ed.* **2010**, *49*, 6260-6266.

16) Kim, M.; Cahill, J. F.; Su, Y.; Prather, K. A.; Cohen, S. M. Postsynthetic ligand exchange as a route to functionalization of 'inert' metal—organic frameworks. *Chem. Sci.* **2012**, *3*, 126-130.

17) Karagiaridi, O.; Bury, W.; Sarjeant, A. A.; Stern, C. L.; Farha, O. K.; Hupp, J. T. Synthesis and characterization of isostructural cadmium zeolitic imidazolate frameworks via solvent-assisted linker exchange. *Chem. Sci.* **2012**, *13*, 3256-3260.

18) Huang, X.-C.; Lin, Y.-Y.; Zhang, J.-P.; Chen, X.-M. Ligand-Directed Strategy for Zeolite-Type Metal—Organic Frameworks: Zinc(II) Imidazolates with Unusual Zeolitic Topologies. *Angew. Chem. Int. Ed.* **2006**, *45*, 1557-1559.

19) Fei, H.; Cahill, J. F.; Prather, K. A.; Cohen, S. M. Tandem Postsynthetic Metal Ion and Ligand Exchange in Zeolitic Imidazolate Frameworks. *Inorg. Chem.* **2013**, *52*, 4011-4016.

20) Banerjee, R.; Phan, A.; Wang, B.; Knobler, C.; Furukawa, H.; O'Keeffe, M.; Yaghi, O. M. High-throughput synthesis of zeolitic imidazolate frameworks and application to CO_2 capture. *Science* **2008**, *319*, 939-943.

Chapter 5

Conclusion and Future Directions

5.1 Summary

The work presented herein provides an examination of different facets of functionality and functionalization in metal—organic frameworks (MOFs). MOFs have been explored in the literature for applications in gas storage, separations, and catalysis among others.[1-3] One such example is the use of MOFs for the purification of MeCl described in Chapter 2. MOFs possessing coordinatively unsaturated metal sites have shown great potential for the purification of MeCl by sorption of DME. This offers a replacement for current industrial purification methods that rely on reactive separations. The three MOFs tested possessing coordinatively unsaturated metal centers were able to remove a significant quantity of DME diluted in a stream of MeCl largely due to the coordinatively unsaturated metal centers that selectively bind to DME. Among these MOFs, Co/DOBDC had a nearly 5-fold higher total capacity and 3-fold higher breakthrough capacity for DME than silica gel and other conventional adsorbents. Additionally, Co/DOBDC was also easily regenerated under mild conditions and still maintained a high total capacity for DME. MOFs are able to provide a significant improvement over previously examined sorptive materials and should provide for a more environmentally and economically efficient purification method than the currently utilized sulfuric acid scrubbing.

Chapter 3 focused on determining the distribution of ligands throughout the MOF structure after ligand exchange. Postsynthetic ligand exchange (PSE) has been implicated as a method for the incorporation of functional groups into MOFs and is widely used in the field due to its mild reaction conditions and generally widespread applicability.[4-8] In these uses, ligand distribution has never been thoroughly examined leaving to question the relative positions of functional groups throughout the MOF especially in cases where PSE is incomplete. Examination of MOFs after PSE in the work presented here has shown strong core-shell architectures naturally arising within MOF-5, UMCM-8, and UiO-66. All three examples

showed incorporation of BDC-d_4 first at the surface and then, after additional time, extending in towards the center. This occurs due to the slow diffusion of the carboxylic acid ligand into the pores of the MOF allowing for exchange to occur faster than the diffusion contrary to the commonly held notion that the large pore sizes of MOFs should not restrict guest diffusion. The perfection of the shells on, at least, the micron level is excellent and exceeds that available from epitaxial overgrowth with the additional advantage that concomitant nucleation and growth of pure phases does not compete with shell formation. The shell structure is absolutely advantageous for concentrating catalytic sites on the outer surfaces of MOF crystals as well as for controlled guest access to the core for selective separations. Other systems are currently being examined to understand the microstructure of PSE in MOFs with different ligand coordination environments and linkers with different topicity (*vide infra*).

Chapter 4 sought to take advantage of PSE in the incorporation of a primary amine moiety into zeolitic imidazolate frameworks (ZIFs) where a more straightforward incorporation method would not be sufficient. PSE was used to incorporate histamine, a primary amine bearing imidazole, into a prototypical ZIF, ZIF-8. The modified material Hist@ZIF-8 was shown to have improved CO_2 capacity compared to the parent ZIF-8 and in particular showed dramatic low pressure uptake that is commensurate with a chemisorptive process similar to other primary amine based CO_2 sorbents. This has shown the potential for histamine to be utilized in the synthesis and design of ZIFs allowing for tailoring towards CO_2 capture or potentially other small molecule. Incorporation of histamine into a ZIF possessing a larger pore would be desirable as it would allow for selective adsorption of other large molecules such as chemical warfare agents. Attempts at modifying another ZIF, ZIF-70, with histamine has been challenging thus far due to the presumed reactivity of the primary amine on the linker. Protecting the primary amine with acetyl and t-butoxycarbonyl moieties to stymie reactivity allowed for successful incorporation of these modified histamines into ZIF-70. Attempts at removing the protecting groups after incorporation into ZIF-70 are ongoing (*vide infra*).

5.2 Future Work

Ligand exchange has proven to be a useful tool in the development of MOFs with different functionalities and, with the MOFs shown above, MOFs with a core-shell distribution of functionalities. Currently, this core-shell structure via PSE is only known for the MOFs

described in Chapter 3 and other systems would need to be studied to find if this finding has more widespread applicability. Specifically, the systems examined only have focused on terephthalic acid which, while one of the most important linkers, is a component of only a small fraction of known MOFs. Expanding this work to MOFs that utilize different linkers such as extended linear linkers or tritopic linkers (or other polytopic linker) would be beneficial toward understanding the mechanism and utility of PSE. Extended linear linkers are expected to behave similarly to the MOFs above with perhaps the only difference coming from the effect of increased pore aperture potentially allowing the ligands to diffuse further into the pores; however, during MOF formation with longer linear linkers, interpenetration of MOF lattices can occur which will not only cause pore aperture to decrease but may also result in other complications with the exchange process.[9] Regardless, this is a direction of interest as larger surface area materials are typically desired for applications in gas storage and separations. Polytopic linkers are likewise of interest as we are not aware of exchange reactions reported with MOFs containing tritopic or higher coordinating linkers. Initial studies would then have to focus on if the exchange is possible before moving to determine the microstructure of the material. The exchange reaction would be expected to take longer in these MOFs with polytopic linkers as three different metal binding groups must be displaced in before complete exchange occurs and as the exchange is reversible, it is possible that even three connection points is too many for ligand exchange to occur. Efforts on exchange in tritopic systems are currently underway using MOF-177 and 1,3,5-tris(4-carboxyphenyl)-2,4,6-trideuterobenzene in a manner similar to the studies in Chapter 3 with MOF-5 and 2,3,5,6-tetradeuteroterephthalic acid (H_2BDC-d_4).[10]

Incorporation of histamine into ZIF-8 has shown a marked improvement of the CO_2 uptake of the material. The presence of primary amines lining the pores of the MOF can be advantageous for other applications such as selective separations and uptake. One such area of focus would be in the uptake and capture of chemical warfare agents (CWAs). For such applications, ZIF-8 presents imitations due to its small pore aperture (~3.4 Å).[11] Incorporation of histamine into a large pore ZIF is a desirable approach to address this issue. The primary amine causes degradation of ZIF-70 upon attempts at PSE as denoted in Chapter 4. To this end, protected histamines present a promising pathway for incorporation of the primary amine. With the primary amine protected, the ligand was successfully incorporated and deprotection studies proceeded and did not ultimately result in revealing the primary amine. Further advancement

towards incorporation of histamine into ZIFs diverges into a number of paths. While PSE was explored here exclusively for the incorporation of histamine or its protected forms, it is possible to conceive of a pathway for inclusion that uses these ligands in direct synthesis of the ZIFs in question. While histamine on its own is expected to be problematic for solvothermal ZIF synthesis, its derivatives are promising in this regard. The groups of Telfer and Kaskel have both shown that despite the thermal sensitivity of t-butoxycarbonyl protected amine, this protecting group is stable to a number of solvothermal conditions used in MOF synthesis.[12,13] It is thus likely that conditions for direct incorporation of boc-protected histamine through solvothermal methods exist and this would provide for a straightforward method towards integration of histamine into other ZIFs. Though in this case with the protected amines, deprotection strategies would need to be explored.

Another option for incorporation of histamine into ZIFs is through other direct MOF syntheses. In particular, liquid assisted grinding has seen rise in usage as a method of synthesizing MOFs at lower temperatures than with standard solvothermal conditions.[14] Ball-milling of the ligands and zinc oxide can form a number of different ZIFs though histamine may have the same issues with MOF formation due to the primary amine.[15] This would provide a facile method for incorporation into different ZIFs or may allow for the formation of new materials.

5.3 References

1) He, Y.; Zhou, W.; Qian, G.; Chen, B. Methane storage in metal—organic frameworks. *Chem. Soc. Rev.* **2014**, *43*, 5657-5678.

2) Trickett, C. A.; Helal, A.; Al-Maythalony, B. A.; Yamani, Z. H.; Cordova, K. E.; Yaghi, O. M. The chemistry of metal—organic frameworks for CO2 capture, regeneration and conversion. *Nature Reviews Materials* **2017**, *2*, 17045.

3) Huang, Y.-B.; Liang, J.; Wang, X.-S.; Cao, R. Mulitfunctional metal—organic framework catalysts: synergistic catalysis and tandem reactions. *Chem. Soc. Rev.* **2017**, *46*, 126-157.

4) Burnett, B. J.; Barron, P. M.; Hu, C.; Choe, W. Stepwise Synthesis of Metal—Organic Frameworks: Replacement of Structural Organic Linkers. *J. Am. Chem. Soc.* **2011**, *133*, 9984-9987.

5) Kim, M.; Cahill, J. F.; Su, Y.; Prather, K. A.; Cohen, S. M. Postsynthetic ligand exchange as a route to functionalization of 'inert' metal—organic frameworks. *Chem. Sci.* **2012**, *3*, 126-130.

6) Karagiaridi, O.; Bury, W.; Sarjeant, A. A.; Stern, C. L.; Farha, O. K.; Hupp, J. T. Synthesis and characterization of isostructural cadmium zeolitic imidazolate frameworks via solvent-assisted linker exchange. *Chem. Sci.* **2012**, *13*, 3256-3260.

7) Xu, Y.; Vermeulen, N. A.; Liu, Y.; Hupp, J. T.; Farha, O. K. SALE-Ing a MOF-Based "Ship of Theseus." Sequential Building-Block Replacement for Complete Reformulation of a Pillared-Paddlewheel Metal—Organic Framework. *Eur. J. Inorg. Chem.* **2016**, 4345-4348.

8) Li, T.; Kozlowski, M. T.; Doud, E. A.; Blakely, M. N.; Rosi, N. L. Stepwise Ligand Exchange for the Preparation of a Family of Mesoporous MOFs. *J. Am. Chem. Soc.* **2013**, *135*, 11688-11691.

9) Eddaoudi, M.; Kim, J.; Rosi, N.; Vodak, D.; Wachter, J.; O'Keeffe, M.; Yaghi, O. M. Systematic Design of Pore Size and Functionality in Isoreticular MOFs and Their Application in Methane Storage. *Science* **2002**, *295*, 469-472.

10) Chae, H. K.; Siberio-Perez, D. Y.; Kim, J.; Go, Y.; Eddaoudi, M.; Matzger, A. J.; O'Keeffe, M.; Yaghi, O. M. A Route to High Surface Area, Porosity and Inclusion of Large Molecules in Crystals. *Nature* **2004**, *427*, 523-527.

11) Banerjee, R.; Phan, A.; Wang, B.; Knobler, C.; Furukawa, H.; O'Keeffe, M.; Yaghi, O. M. High-throughput synthesis of zeolitic imidazolate frameworks and application to CO_2 capture. *Science* **2008**, *319*, 939-943.

12) Lun, D. J. Waterhouse, G. I. N.; Telfer, S. G. A General Thermolabile Protecting Group Strategy for Organocatalytic Metal—Organic Frameworks. *J. Am. Chem. Soc.* **2011**, *133*, 5806-5809.

13) Padmanaban, M.; Muller, P.; Lieder, C.; Gedrich, K.; Grunker, R.; Bon, V.; Senkovska, I.; Baumgartner, S.; Opelt, S.; Paasch, S.; Brunner, E.; Glorius, F.; Klemm, E.; Kaskel, S. Application of a chiral metal—organic framework in enantioselective separation. *Chem. Commun.* **2011**, *47*, 12089-12091.

14) Friscic, T.; Reid, D. G.; Halasz, I.; Stein, R. S.; Dinnebier, R. E.; Duer, M. J. Ion- and Liquid-Assisted Grinding: Improved Mechanochemical Synthesis of Metal—Organic Frameworks Reveals Salt Inclusion and Anion Templating. *Angew. Chem. Int. Ed.* **2009**, *49*, 712-715.

15) Katsenis, A. D.; Puskaric, A.; Strukil, V.; Mottillo, C.; Julien, P. A.; Uzarevic, K.; Pham, M.-H.; Do, T.-O.; Kimber, S. A. J.; Lazic, P.; Magdysyuk, O.; Dinnebier, R. E.; Halasz, I.; Friscic, T. *In situ* X-ray diffraction monitoring of a mechanochemical reaction reveals a unique topology metal-organic framework. *Nat. Commun.* **2015**, *6*.